

N87-28348

NAG 1-703

D2-64

94210

The Jacobi Matrix Technique
in Computational Fluid Dynamics

by

H. Thomas Sharp

S.B., Physics, Massachusetts Institute of Technology, 1981

S.B., Mathematics, Massachusetts Institute of Technology, 1981

S.M., Aero. & Astro., Massachusetts Institute of Technology, 1983

M.Sc., Applied Mathematics, Brown University, 1985

Thesis

Submitted in partial fulfillment of the requirements for the
Degree of Doctor of Philosophy in the Division of
Applied Mathematics at Brown University

May 1988

Copyright

by

H. Thomas Sharp

1988

This dissertation by H. Thomas Sharp
is accepted in its present form by the Division of
Applied Mathematics as satisfying
dissertation requirement for the degree of Doctor of Philosophy

Date _____
Lawrence Sirovich

Recommended to the Graduate Council

Date _____
Frederic E. Bisshopp

Date _____
David Gottlieb

Approved by the Graduate Council

Date _____

VITA

H. Thomas Sharp was born on [REDACTED] in [REDACTED]. He earned undergraduate degrees in physics and mathematics from MIT in 1981. While an undergraduate, he learned to fly and received his pilot's license in 1981. Wanting to learn more about aerodynamics, he stayed at MIT and studied computational aerodynamics in the Department of Aeronautics and Astronautics receiving a Master's degree in 1983. In the fall of 1983 he entered Brown University to study fluid dynamics in the Division of Applied Mathematics and received a Master's degree in 1985. Upon his graduation from Brown in the summer of 1987 he started working as an aerodynamicist for Lockheed-California Co..

Acknowledgements

It is with great pleasure that the author wishes to express his sincere appreciation and thanks to the following people:

Professor Lawrence Sirovich not only for suggesting the topic and providing the guidance throughout the course of this work, but also for his patience and understanding during my stay at Brown.

Professors Frederic Bisshopp and David Gottlieb for evaluating this manuscript and for their lucid explanations of and help with understanding computational fluid dynamics.

Ms. Andria Durk and Ms. Madeline Brewster for typing the seemingly endless revisions of this dissertation.

Most of all I would like to thank my parents. Their encouragement and assistance made this degree possible.

CONTENTS

Vita	iii
Acknowledgments	iv
Introduction	1
Chapter 1, The Jacobi Matrix Technique and It's Application to Two-Dimensional Supersonic Flow	3
Application to 2D Supersonic Flow	4
Variational Equations	6
Results	8
Inverse Case	9
Figure Captions	11
Figures	12
References	20
Chapter 2, The Application of the Jacobi Matrix Technique to Axisymmetric Supersonic Flow	21
Application to Axisymmetric Supersonic Flow	22
Variational Equations	24
Results	26
Inverse Case	26
Figure Captions	28
Figures	29
References	34
Chapter 3, The Jacobi Matrix Technique for General Flows	35
Direct Differencing	36
2D Subsonic Flow	38
Calculation of the Jacobi Matrix	41
Results	41
Figure Captions	43
Figures	44
References	53

INTRODUCTION

Flow past a body is, in general, specified by a variety of parameters such as thickness, angle of attack, camber, Mach number etc. A particular flow is, therefore, characterized by a single point in the corresponding parameter space. Conversely, the numerical calculation of a particular flow field yields information at just one point of the parameter space. However, the nature of a continuous range of nearby flow fields is of fundamental significance in the design and performance of aircraft. To treat this generally, one can consider the variational equations (which are linear) obtained by differentiating the exact equations with respect to each of the relevant parameters. The resulting matrix of derivatives of flow quantities is referred to as the Jacobi matrix.

The subsequent procedure is, in principle, straightforward. One integrates the nonlinear governing equations -- which results in the determination of just one point in parameter space -- and simultaneously the variational equations governing the Jacobi matrix. The last is then used to describe the neighborhood of the already determined point of the parameter space. A method is presented herein which allows efficient generation of solutions in the neighborhood of a base solution. Since the variational equations are linear, the additional computational time required for their integration is modest.

We have applied the Jacobi matrix technique to the direct calculation of inviscid supersonic flow about

- o two dimensional airfoils of varying thickness, angle of attack and camber
- o axisymmetric bodies of varying thickness and taper

and the design (inverse) calculation of inviscid supersonic flow past

- o airfoils described by a given family of pressure distributions
- o axisymmetric bodies described by a given family of pressure distributions.

Also we applied the method to subsonic potential flow about two dimensional

airfoils by modifying Jameson's FLO36.

Results of our calculations show that the Jacobi method allows for the efficient and accurate generation of parametric solutions in the neighborhood of a known solution. In general terms, we consider a system of nonlinear partial differential equations

$$\underline{F}(\underline{u}(\underline{x};\underline{\epsilon}), \underline{x};\underline{\epsilon}) = 0 \quad (I.1)$$

in the flow variables \underline{u} , dependent variables \underline{x} , and parameters $\underline{\epsilon}$. For purposes of exposition we regard $\underline{u}(\underline{x};\underline{\epsilon})$ as known and seek the solution at a neighboring point in parameter space. The parametrically differentiated dependent variables are governed by the equations obtained by differentiating (1), viz.

$$\frac{d}{d\epsilon_k} F_i(\underline{u}, \underline{x}; \underline{\epsilon}) = \frac{\partial F_i}{\partial u_j} \frac{\partial u_j}{\partial \epsilon_k} + \frac{\partial F_i}{\partial \epsilon_k} = 0 \quad (I.2)$$

The, in general, non-square matrix $\frac{\partial u_i}{\partial \epsilon_k}$ is known as the Jacobi matrix and the above procedure provides a linear system of equations governing the Jacobi matrix. The term $\partial F_i / \partial u_j$ actually represents an operator, the details of which are best left to the individual cases. If $\underline{u}^0 = \underline{u}(\underline{x}; \underline{\epsilon}_0)$ represents a known solution of the flow then any neighboring flow at some fixed point \underline{x} is determined by

$$\underline{u}(\underline{x}; \underline{\epsilon}) \approx \underline{u}^0 + \frac{\partial \underline{u}^0}{\partial \underline{\epsilon}_k} (\underline{\epsilon}_k - \underline{\epsilon}_0) \quad (I.3)$$

In what follows we will be somewhat loose in not distinguishing between the two sides of (I.3). A basic difficulty with what has been just said, in particular to the use of (I.3), is the fact that the conditions on the problem occur at locations which vary with $\underline{\epsilon}$. Specifically, both the boundary locations (and shock locations) may vary with changes in the parameters $\underline{\epsilon}$. We first present a method that avoids the difficulties implicit in such spatial variations with $\underline{\epsilon}$, and later treat directly the formulation implicit in (I.1-3).

Chapter I
The Jacobi Matrix Technique and
It's Application to Two-Dimensional
Supersonic Flow

The White Rabbit put on his spectacles. "Where shall I begin, please your Majesty?" he asked.

"Begin at the beginning," the King said, very gravely, "and go on till you come to the end: then stop."

- Alice's Adventures in Wonderland
Lewis Carroll

APPLICATION TO 2D SUPERSONIC FLOW

To illustrate this method we consider steady, inviscid, supersonic flows past two dimensional airfoils. For this purpose and in order to be specific, consider a family of profiles depending on three parameters (thickness, camber, and angle of attack). For completeness, we summarize the methods used in solving such flows [1], [2]. The equations are written in characteristic form as follows:

$$s_{\beta} = 0 \quad (1.1)$$

$$(\theta + P(\mu))_{\alpha} = \frac{\sin 2\mu}{2\gamma} s'(\alpha) \quad (1.2)$$

$$(\theta - P(\mu))_{\beta} = (1 - \tan\theta \tan\mu) \frac{x_{\beta}}{x_{\alpha}} \theta_{\alpha} \quad (1.3)$$

Here the coordinates (α, β) correspond to the streamlines, $\alpha = \text{constant}$, and the C^+ characteristics, $\beta = \text{constant}$ (Figure 1). θ is the flow deflection angle, μ is the Mach angle and s is the entropy. $P(\mu)$ is the Prandtl function given by

$$P(\mu) = \lambda^{\frac{1}{2}} \tan^{-1} (\lambda^{\frac{1}{2}} \tan\mu) - \mu, \quad \lambda = (\gamma + 1) / (\gamma - 1). \quad (1.4)$$

An advantage to solving the above characteristic form of the equations is that it generates a body fit, shock fit coordinate system. We mention in passing that since the equations are exact, they are valid in the hypersonic flow regime so long as such real gas effects as disassociation and ionization can be ignored.

The physical coordinates x, y satisfy the relations [1], [2]

$$y_{\alpha} = x_{\alpha} \tan(\theta + \mu), \quad y_{\beta} = x_{\beta} \tan\theta \quad (1.5)$$

The transformation to (α, β) coordinates leaves open two arbitrary functions and these are fixed so that the shock is along $\alpha = \beta$ and the airfoil is positioned along the line $\alpha = 0$ (Figure 2). Appropriate boundary conditions at the body are

$$x(0, \beta) = \beta, \quad y(0, \beta) = f(\beta, \underline{\epsilon}), \quad \theta(0, \beta) = \tan^{-1}(f_{\beta}(\beta, \underline{\epsilon})). \quad (1.6)$$

The Rankine-Hugoniot conditions govern the jumps in θ , μ and s at the shock.

Written in terms of the shock angle η , they are given by

$$\tan \theta = \frac{1}{\tan \eta} \frac{(M^2 - 1) \tan^2 \eta - 1}{\left(1 + \frac{\gamma - 1}{2} M^2\right) + \left(1 + \frac{\gamma - 1}{2} M^2\right) \tan^2 \eta} \quad (1.7)$$

$$\sin^2 \mu = \frac{0.2(1 + \frac{7}{6}w)(1 + \frac{1}{6}w)}{(1+w)(1 + 0.2M^2) - (1 + \frac{7}{6}w)(1 + \frac{1}{6}w)} \quad (1.8)$$

$$s = 2.5 \ln \left(1 + \frac{7}{6}w\right) + 3.5 \ln \left(1 + \frac{1}{6}w\right) - 3.5 \ln (1+w) \quad (1.9)$$

where

$$w = M^2 \sin^2 \eta - 1 \quad (1.10)$$

The shock angle is related to the coordinates as follows

$$\tan \eta = \left. \frac{dy}{dx} \right|_{\text{shock}} = \frac{y_{\alpha} + y_{\beta}}{x_{\alpha} + x_{\beta}} \Big|_{\text{shock}} \quad (1.11)$$

In the above we have assumed a perfect gas with constant specific heats and hence that

$$p = \rho^{\gamma} \exp [(\gamma - 1)s] \quad (1.12)$$

It should be noted that this formulation eliminates the difficulty mentioned in the Introduction. Namely, by using the (α, β) - coordinate system, a quantity such as

$$\frac{\partial p}{\partial \underline{\epsilon}}(\alpha, \beta; \underline{\epsilon})$$

signifies the variation with $\underline{\epsilon}$ at fixed α and β . In particular it gives the variation of pressure say fixed at the body, $\alpha = 0$, or at the shock, $\alpha = \beta$. This makes the integration of the differential equations significantly simpler.

VARIATIONAL EQUATIONS

We are interested in solutions to these equations at points near a known solution. To pursue this we differentiate all of the above equations with respect to a typical parameter of interest. In keeping with the remarks at the close of the previous section, we emphasize that differentiation is with respect to $\underline{\epsilon}$ with α and β held fixed.

The mechanics of the differentiation are straightforward but tedious. We represent by capitalized variables the differentiated variables;

$$\Theta = \frac{\partial \theta}{\partial \epsilon}, \quad S = \frac{\partial s}{\partial \epsilon}, \quad X = \frac{\partial x}{\partial \epsilon}, \quad Y = \frac{\partial y}{\partial \epsilon}, \quad \Psi = \frac{\partial \mu}{\partial \epsilon} \quad (1.13)$$

when (1.4), (1.5), (1.6), and (1.8) are parametrically differentiated we obtain,

$$S_{\beta} = 0 \quad (1.14)$$

$$\Theta_{\alpha} + [P_{\mu\mu}(\mu) \mu_{\alpha} - \frac{s_{\alpha} \cos 2\mu}{\gamma}] \Psi + P_{\mu}(\mu) \Psi_{\alpha} - \frac{\sin 2\mu}{2} S_{\alpha} = 0 \quad (1.15)$$

$$\Theta_{\beta} + \left[\frac{x_{\beta} \theta_{\alpha}}{x_{\alpha}} \sec^2 \theta \tan \mu \right] \Theta - (1 - \tan \theta \tan \mu) \frac{x_{\beta}}{x_{\alpha}} \Theta_{\alpha} =$$

$$P_{\mu}(\mu) \Psi_{\beta} + [P_{\mu\mu}(\mu) \mu_{\beta} - \frac{x_{\beta} \theta_{\alpha}}{x_{\alpha}} \sec^2 \mu \tan \theta] \Psi + (1 - \tan \theta \tan \mu) \frac{\theta_{\alpha}}{x_{\alpha}} (X_{\beta} - \frac{x_{\beta}}{x_{\alpha}} X_{\alpha}) \quad (1.16)$$

$$Y_{\alpha} = X_{\alpha} \tan(\theta + \mu) + X_{\alpha} \sec^2(\theta + \mu)(\Theta + \Psi) \quad (1.17)$$

$$Y_{\beta} = X_{\beta} \tan \theta + X_{\beta} \sec^2 \theta \quad (1.18)$$

It should be noted that we have dropped the specification that ϵ be a vector. This has been done for ease of exposition. This can be done without loss of generality. Variation with respect to each parameter can be treated separately, since only first order variations are being considered.

At the shock the parametrically differentiated equations are

$$\frac{d\eta}{d\epsilon} = \frac{\cos 2\eta}{(x_\alpha + x_\beta)^2} \left[Y_\alpha(x_\alpha + x_\beta) + Y_\beta(x_\alpha + x_\beta) - X_\alpha(y_\alpha + y_\beta) - X_\beta(y_\alpha + y_\beta) \right] \quad (1.19)$$

$$S = \left[\frac{17.5}{6+7w} + \frac{3.5}{6+w} - \frac{3.5}{1+w} \right] \frac{dw}{d\epsilon} \quad (1.20)$$

$$\Psi = \frac{0.2A \left(\frac{4}{3} + \frac{7}{18} w \right) - 0.2 \left(1 + \frac{7}{6} w \right) \left(1 + \frac{1}{6} w \right) \left(0.2 M^2 - \frac{1}{3} - \frac{7}{18} w \right)}{A^2 \sin 2\mu} \frac{dw}{d\epsilon} \quad (1.21)$$

where $\frac{dw}{d\epsilon} = M^2 \sin 2\eta \frac{d\eta}{d\epsilon}$, $A = 1 + 0.2M^2(1+w) - (1 + \frac{7}{6}w)(1 + \frac{1}{6}w)$

$$\frac{d\theta}{d\epsilon} = \frac{d\eta}{d\epsilon} \cos 2\theta \left\{ \frac{1}{\sin 2\eta} \frac{(M^2-1)\tan^2\eta - 1}{(1 + \frac{\gamma+1}{2} M^2) + (1 + \frac{\gamma-1}{2} M^2) \tan^2\eta} \right. \quad (1.22)$$

$$\left. + \frac{2}{[(1 + \frac{\gamma+1}{2} M^2) + (1 + \frac{\gamma-1}{2} M^2) \tan^2\eta]^2} \left[(M^2 - 1) \sec \eta (1 + \frac{\gamma+1}{2} M^2) \right. \right. \\ \left. \left. + (1 + \frac{\gamma-1}{2} M^2) \tan^2\eta \right] - [(M^2-1)\tan^2\eta - 1] (1 + \frac{\gamma-1}{2} M^2) \sec^2\eta \right\}$$

In the actual integration (1.21-1.25) are applied at the shock

$$\alpha = \beta \quad (1.23)$$

At the body $\alpha = 0$ the appropriate equations are

$$\underline{X} = 0, \quad \underline{Y} = f \frac{\partial \beta}{\partial \epsilon}, \quad \underline{\theta} = \frac{\partial f}{\partial \epsilon} \beta(\beta, \epsilon) \cos^2\theta \quad (1.24)$$

In writing (1.24) we revert to the general case in which many parameters are being considered. At this point we can simultaneously numerically integrate the

non-linear system and the variational equations. The calculation of the base flow is second order accurate [2]. The calculation of the new flow is first order in space, second order in the parameters of interest. The calculation of the two flows is interleaved in that after the flow along $\beta = \text{constant}$ is computed by the base code, the parametric code then calculates the exact derivatives in order to obtain the variational flow.

RESULTS

As we have already mentioned the method applies generally to many independently varying parameters. As a typical use of the variational quantities we use Taylor's theorem to consider the change in pressure,

$$P_{\text{new}} \approx P_{\text{base}} + \sum_i (\partial p / \partial \epsilon_{i0})(\epsilon_i - \epsilon_{i0}) \quad (1.25)$$

where ϵ_i represents the various parameters with the differential coefficients calculated holding α and β fixed and the zero subscript denotes a reference or base calculation.

For example, if just thickness is considered and denoted by say ϵ , then at the body

$$P_{\text{new}} \approx P_{\text{base}} + \left[\frac{\partial p}{\partial \epsilon} \right]_{\alpha=0, \beta} (\epsilon - \epsilon_0) = P_{\text{base}} + \left[\left[\frac{\partial p}{\partial \epsilon} \right]_{x, y=f} \right. \\ \left. + \left[\frac{\partial p}{\partial y} \right]_{x, y=f} \left[\frac{\partial f}{\partial \epsilon} \right] (\epsilon - \epsilon_0) \right] \quad (1.26)$$

The second form exhibits the result obtained if variation in the physical plane is considered.

In the numerical calculations that are discussed, we have taken for f a family of shapes given by

$$y = 2\epsilon x(1-x) - x \tan \Delta + 10x\epsilon(x-1)\left(x - \frac{1}{2}\right)c \quad (1.27)$$

Thus, ϵ is the thickness ratio based on chord, Δ the mean chord angle of attack, and c a scaling factor for the camber (shape) function. Figure 3 shows the effect of changing just the thickness ($\Delta, c = 0$). Here we have plotted the pressure distribution

on the upper surface and the airfoil which, for aesthetic reasons, has the lower surface plotted as a reflection of the upper surface. Note that the method gives good agreement with the exact solution even when the new thickness is fifty percent greater than the base thickness.

More generally we consider variations in all three parameters. Thus, the pressure relation at the body is

$$p_{\text{new}} \approx p_{\text{base}} + \left[\frac{\partial p}{\partial \epsilon} \right]_{\alpha=0, \beta} (\epsilon - \epsilon_0) + \left[\frac{\partial p}{\partial \Delta} \right]_{\alpha=0, \beta} (\Delta - \Delta_0) + \left[\frac{\partial p}{\partial c} \right]_{\alpha=0, \beta} (c - c_0) \quad (1.28)$$

Figures 4 through 6 show the effect of changing various combinations of thickness, angle of attack, and camber. Here we see that, although the airfoil configurations are markedly different, there is very good agreement between the parametrically generated pressure distribution and the exact pressure distribution for the new airfoil.

INVERSE CASE

The method which has been presented also works as well on the inverse or design problem where the pressure on the body is known, but the shape of the body is to be determined. Using the Bernoulli equation and the perfect gas law one may show [1]

$$\mu = \sin^{-1} \left[\left[\frac{\gamma-1}{2} \frac{\exp\left(\frac{\gamma-1}{\gamma} (s + \ln \gamma p)\right)}{1 + \frac{\gamma-1}{2} M^2 - \exp\left(\frac{\gamma-1}{\gamma} (s + \ln \gamma p)\right)} \right]^{\frac{1}{2}} \right] \quad (1.29)$$

This when differentiated, yields

$$\psi = \frac{(\gamma-1)^2}{2\gamma} \frac{\left(1 + \frac{\gamma-1}{2} M^2\right) \exp(w)}{\left[1 + \frac{\gamma-1}{2} M^2 - \exp(w)\right]^2 \sin^2 \mu} S = \frac{(\gamma-1)^2 \left(1 + \frac{\gamma-1}{2} M^2\right) \exp(w)}{2\gamma \left[1 + \frac{\gamma-1}{2} M^2 - \exp(w)\right]^2 \sin^2 \mu} \frac{d(\ln p)}{d\epsilon} \quad (1.30)$$

where

$$w = \frac{\gamma-1}{\gamma} (s + \ln p)$$

Obviously at the airfoil we can no longer use (1.6) since we are hoping to determine the shape of the airfoil. Instead we must use (1.5) and (1.29). Therefore, the parametrically differentiated equations (1.24) must be replaced by (1.17), (1.18) and (1.30). The integration may now proceed as in the direct case [2]. The results of the variational calculations are presented in Figures 7 through 9. Notice that even for a 20% change in the logarithm of the pressure (corresponding to a 50% increase in thickness), the difference between the exact airfoil shape and the computed shape is less than 4%.

FIGURE CAPTIONS

- Fig. 1. Body, C⁺ characteristics, streamlines and C⁻ characteristics (dashed) in physical (x,y) plane, from [1].
- Fig. 2. Body, C⁺ characteristics and streamlines in (α,β) plane.
- Fig. 3. Pressure distribution on 10% and 15% thick airfoils at M = 2 and 10% and 15% airfoils.
- Fig. 4. Pressure distribution on 10% thick airfoil, uncambered at 0 degree angle of attack and cambered (c=0.1) at 5 degrees angle of attack at M = 2 along with respective bodies.
- Fig. 5. Pressure distribution on 10% thick airfoil, uncambered at 0 degree angle of attack and cambered (c=0.2) at 5 degrees angle of attack at M = 2 along with respective bodies.
- Fig. 6. Pressure distribution on 10% thick airfoil, uncambered at 0 degree angle of attack and cambered (c=0.2) at 10 degrees angle of attack at M = 2 along with respective bodies.
- Fig. 7. Inverse case: pressure distribution on 10% and 12% airfoils, M = 2, along with generated bodies. Dashed airfoil is computed shape.
- Fig. 8. Inverse case: pressure distribution on 10% and 15% airfoils, M = 2, along with generated bodies. Dashed airfoil is computed shape.
- Fig. 9. Inverse case: pressure distribution on 10% and 12% airfoils, M = 4, along with generated bodies. Dashed airfoil is computed shape.

PHYSICAL PLANE

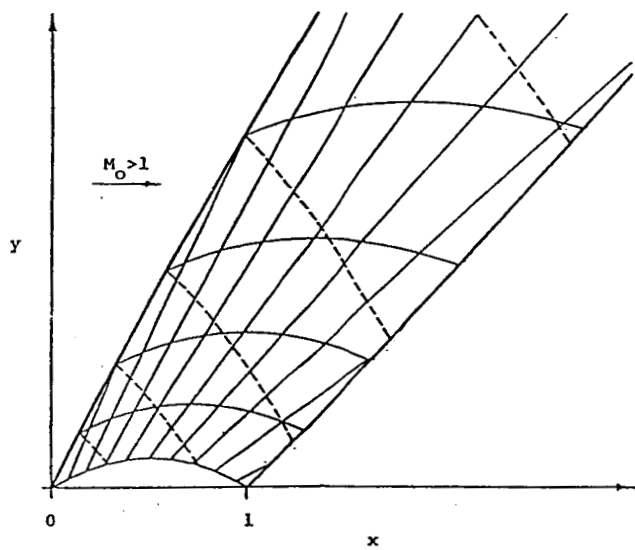


Figure 1

COMPUTATIONAL PLANE

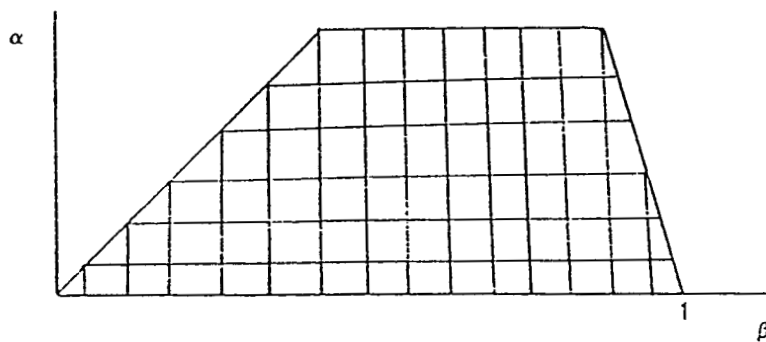


Figure 2

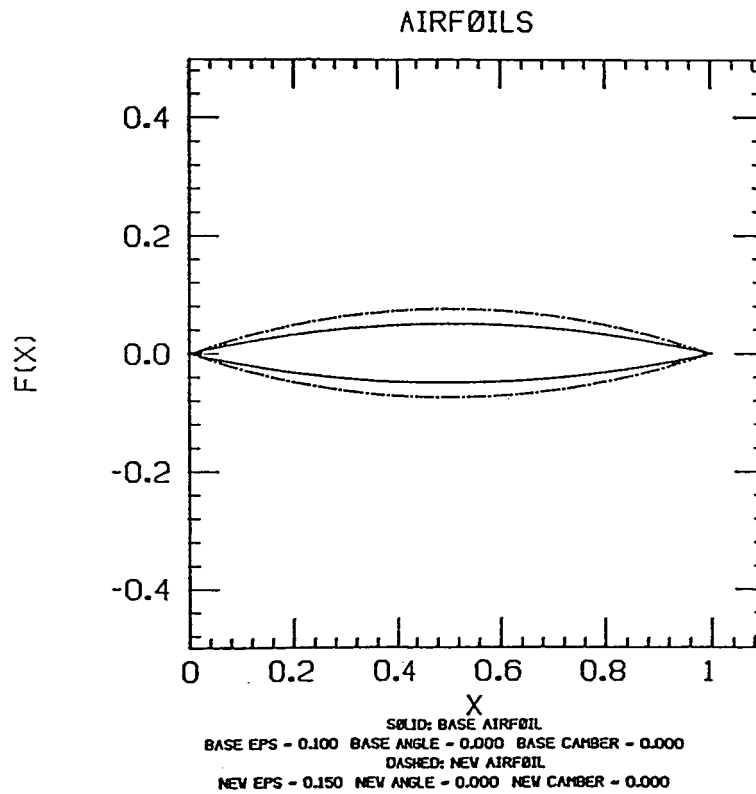
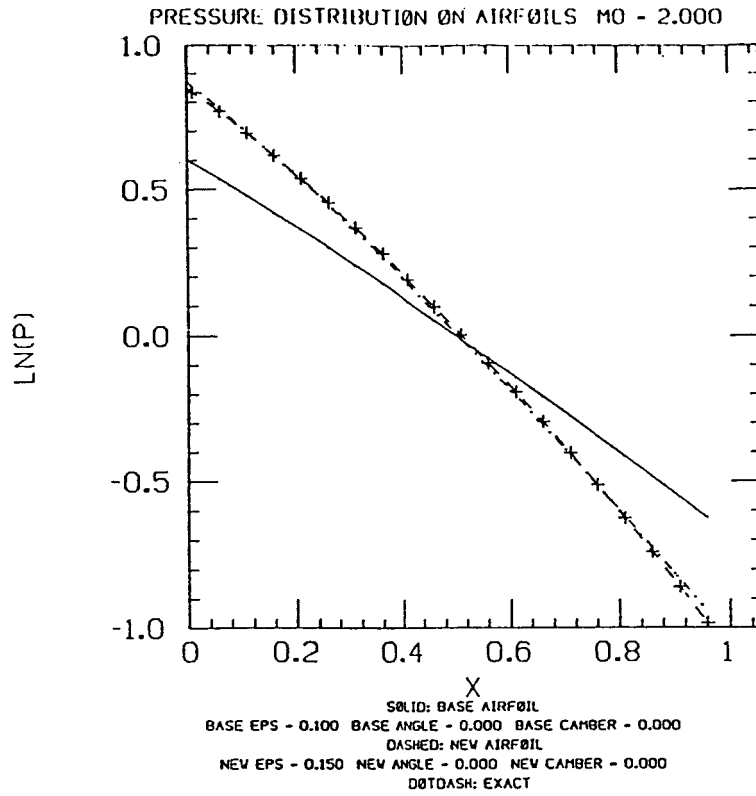


Figure 3

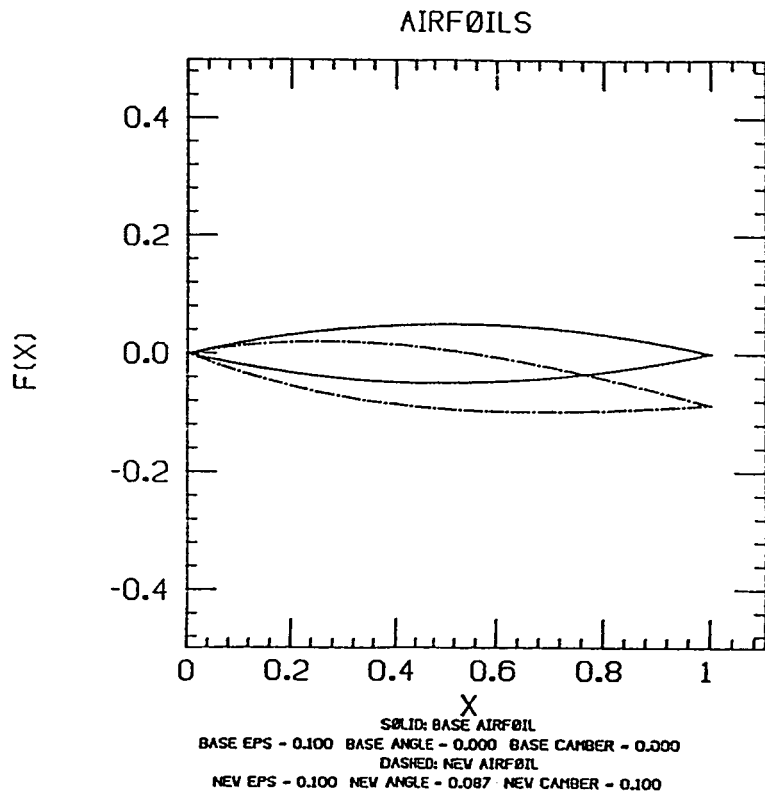
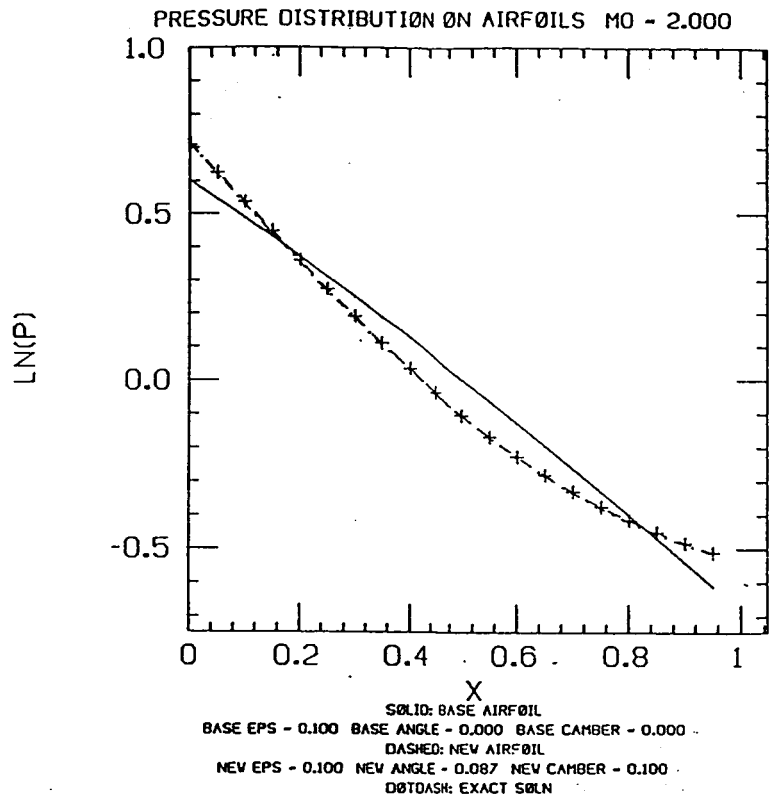


Figure 4

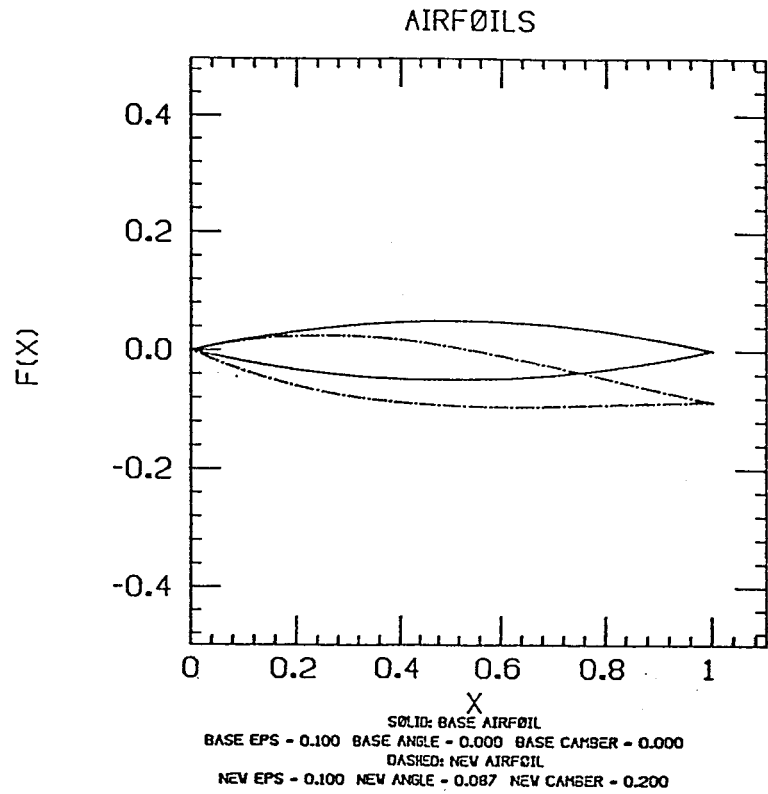
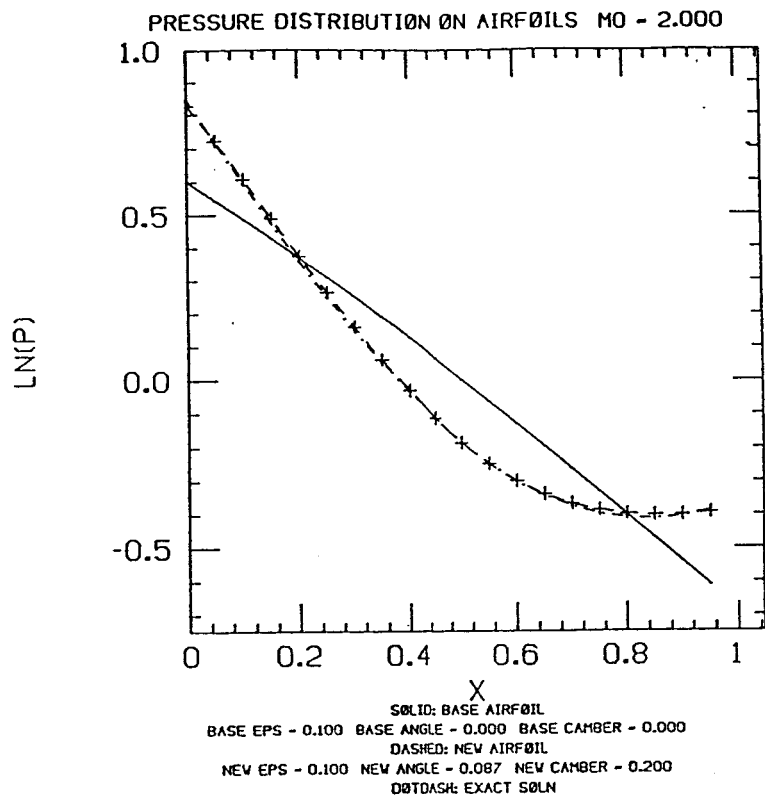


Figure 5

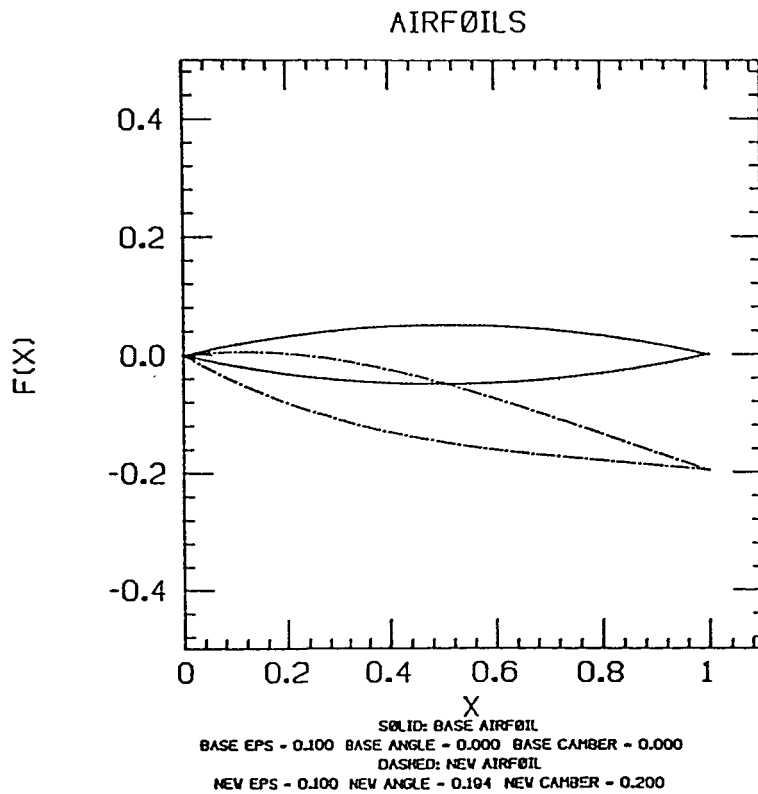
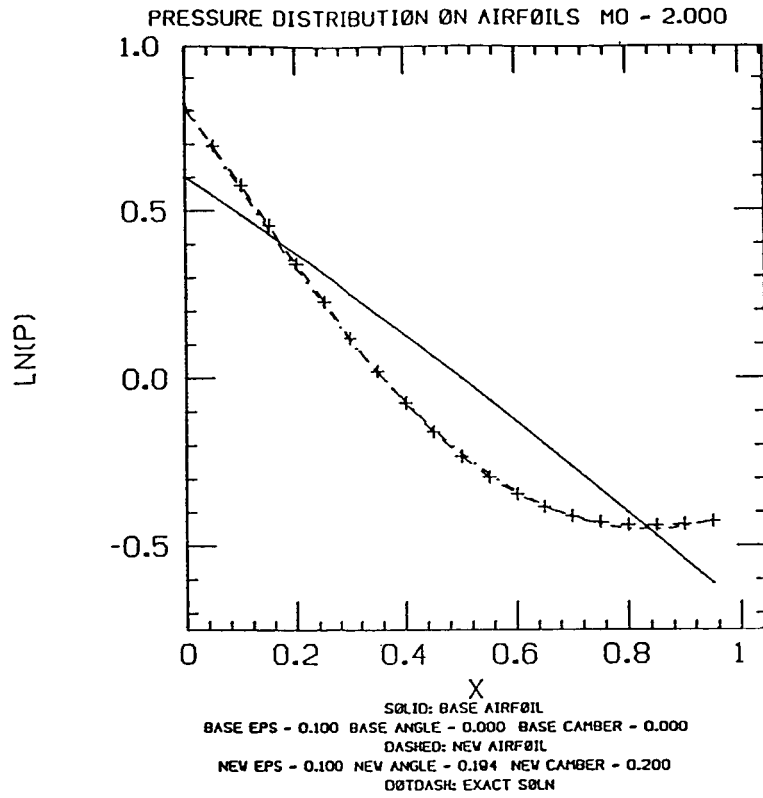


Figure 6

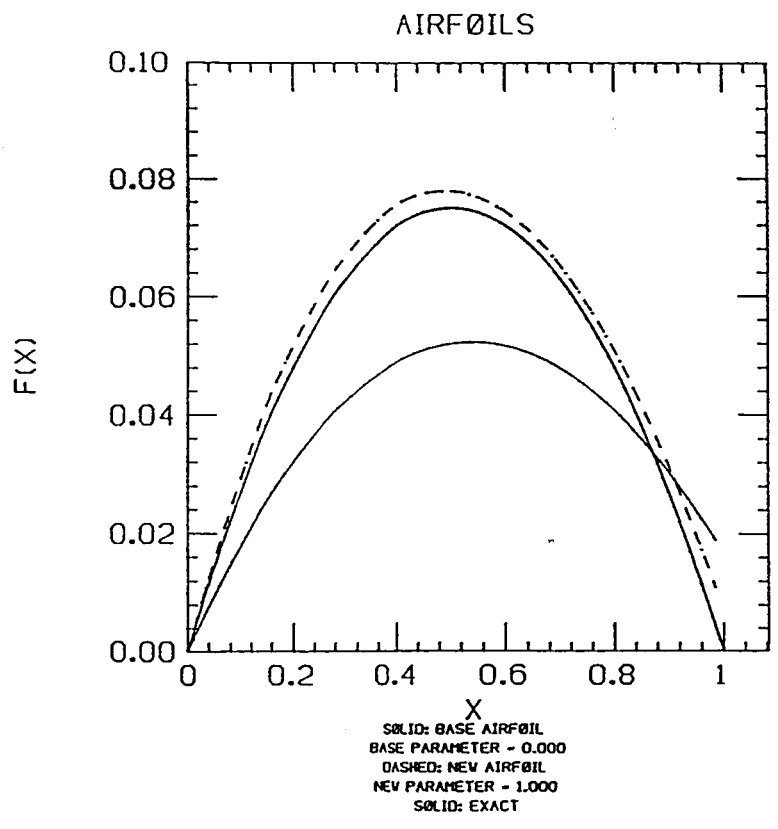
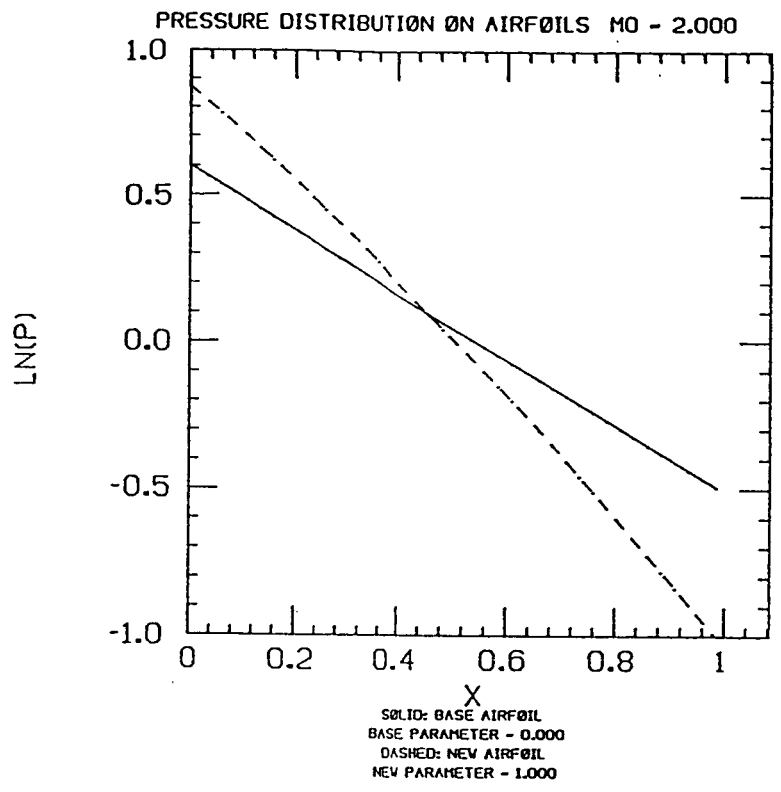


Figure 7

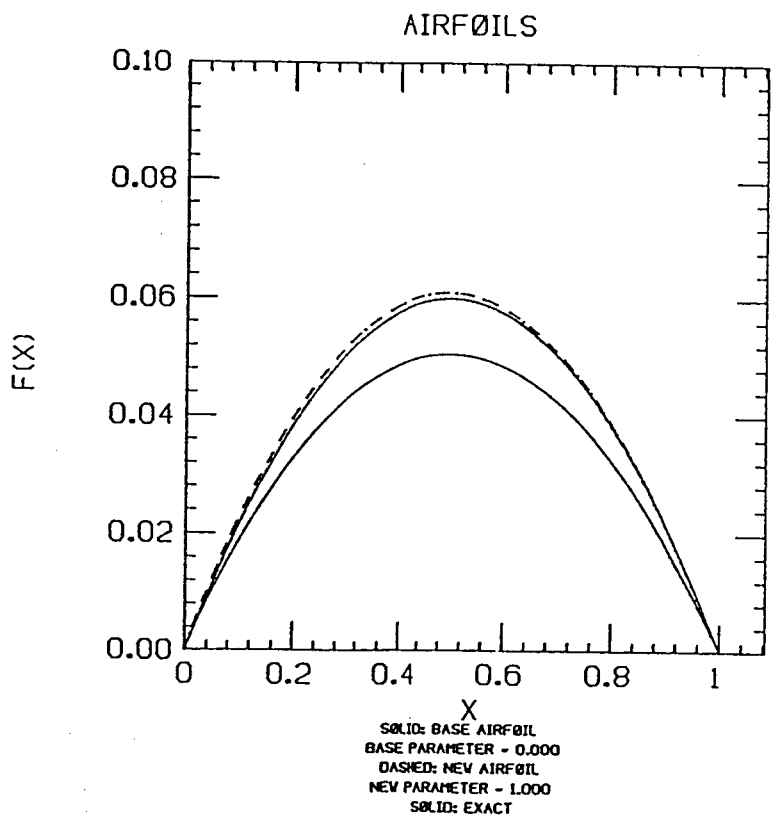
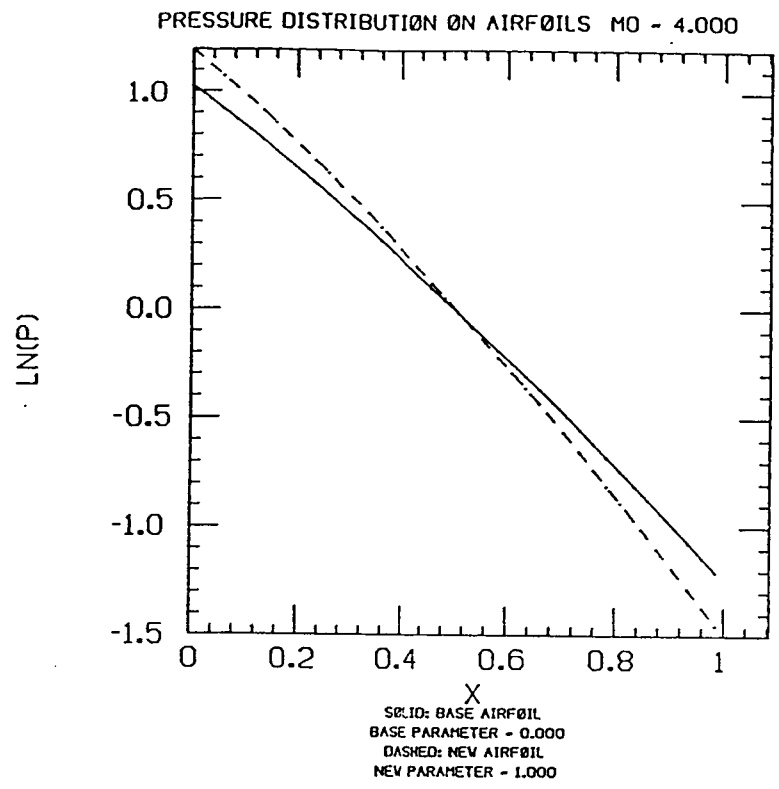
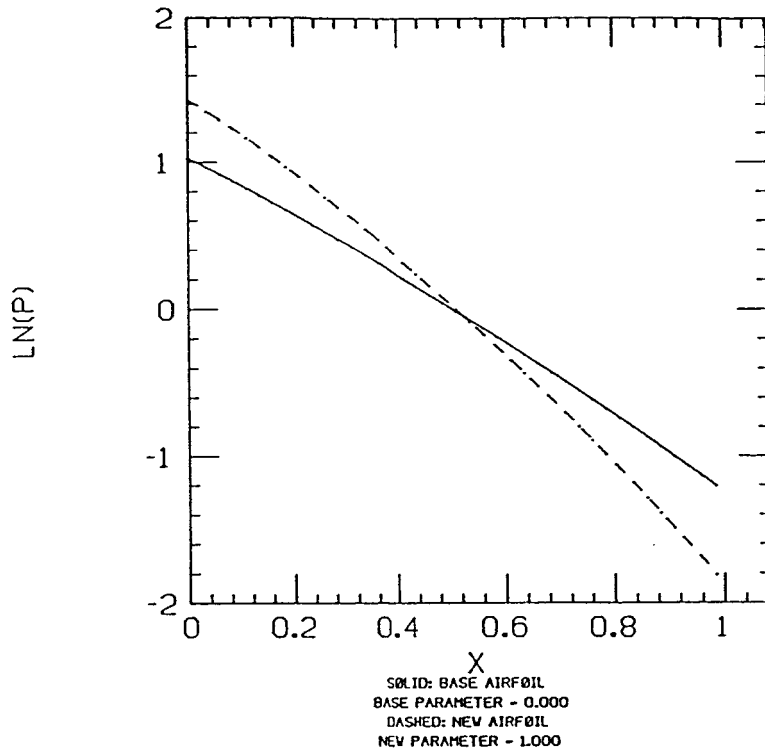


Figure 8

PRESSURE DISTRIBUTION ON AIRFOILS $M_0 = 4.000$



AIRFOILS

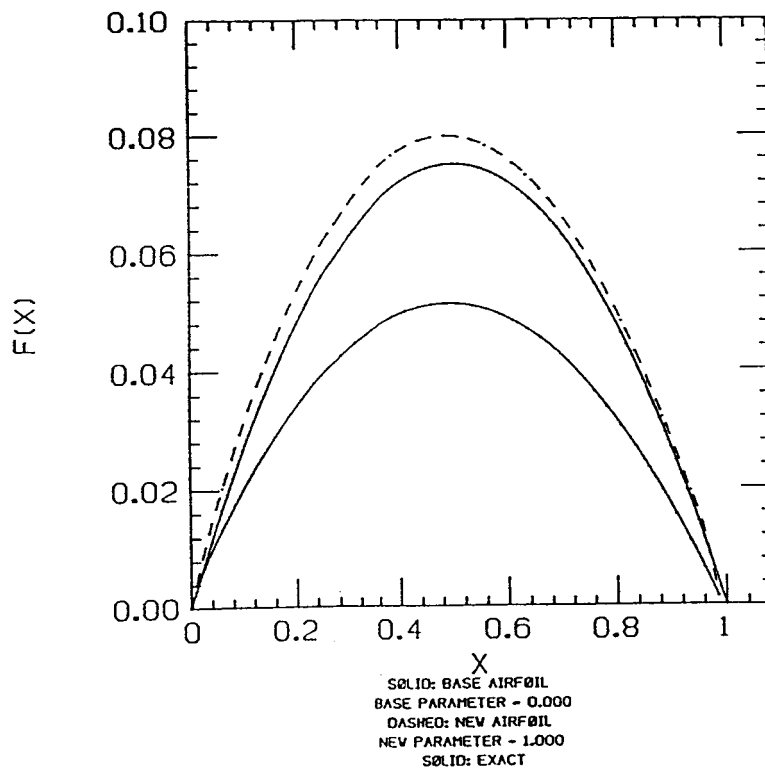


Figure 9

REFERENCES

- [1] Lewis, T.S. and Sirovich, L., "Approximate and Exact Numerical Computation of Supersonic Flow Over an Airfoil", J. Fluid Mechanics Vol 112, 1981, pp. 265-282.

- [2] Fong, J. and Sirovich, L. "Direct and Inverse Problem in Supersonic Axisymmetric Flow", AIAA Journal, 24, 5 May 1986.

Chapter II
The Application of the Jacobi Matrix Technique
to Axisymmetric Supersonic Flow

"Curiouser and curiouser!" cried Alice (she was so much surprised, that for the moment she quite forgot how to speak good English).

- Alice's Adventures in Wonderland
Lewis Carroll

APPLICATION TO AXISYMMETRIC SUPERSONIC FLOW

As another illustration of this method, we consider steady, inviscid, supersonic flows past axisymmetric bodies. For this purpose consider a family of profiles depending on two parameters, thickness and taper. As in Chapter 1, we shall summarize the methods used in solving such flows [1], [2]. The equations are written in characteristic form as follows:

$$s_{\beta} = 0 \quad (2.1)$$

$$(\theta + P(\mu))_{\alpha} = \frac{\sin 2\mu}{2\gamma} s'(\alpha) - \frac{\tan \theta \tan \mu}{\tan \theta + \tan \mu} \frac{r_{\alpha}}{r} \quad (2.2)$$

$$(\theta - P(\mu))_{\beta} = (1 - \tan \theta \tan \mu) \frac{x_{\beta}}{x_{\alpha}} \theta_{\alpha} + \tan \mu \frac{r_{\beta}}{r} \quad (2.3)$$

Here the coordinates (α, β) correspond to the streamlines, $\alpha = \text{constant}$, and the C^+ characteristics, $\beta = \text{constant}$ (Figure 1). θ is the flow deflection angle, μ is the Mach angle and s is the entropy. $P(\mu)$ is the Prandtl function given by

$$P(\mu) = \lambda^{1/2} \tan^{-1} (\lambda^{1/2} \tan \mu) - \mu, \quad \lambda = (\gamma + 1) / (\gamma - 1). \quad (2.4)$$

As in the two-dimensional case, these equations are exact and are valid in the hypersonic flow regime so long as such real gas effects as disassociation and ionization can be ignored. The physical coordinates x, r satisfy the relations [1], [2]

$$r_{\alpha} = x_{\alpha} \tan(\theta + \mu), \quad r_{\beta} = x_{\beta} \tan \theta \quad (2.5)$$

As with Chapter 1, the transformation to (α, β) coordinates leaves open two arbitrary functions; these are fixed so that the shock is along $\alpha = \beta$ and the body is positioned along the line $\alpha = 0$ (Figure 2). Hence, we have a body fit, shock fit coordinate system. The boundary conditions at the body are

$$x(0, \beta) = \beta, \quad r(0, \beta) = f(\beta, \underline{\epsilon}), \quad \theta(0, \beta) = \tan^{-1} (f_{\beta}(\beta, \underline{\epsilon})). \quad (2.6)$$

The Rankine-Hugoniot conditions govern the jumps in θ , μ and s at the shock. Written in terms of the shock angle η , they are given by

$$\tan\theta = \frac{1}{\tan\eta} \frac{(M^2 - 1) \tan^2\eta - 1}{(1 + \frac{\gamma+1}{2} M^2) + (1 + \frac{\gamma-1}{2} M^2) \tan^2\eta} \quad (2.7)$$

$$\sin^2\mu = \frac{0.2(1 + \frac{7}{6}w)(1 + \frac{1}{6}w)}{(1+w)(1+0.2M^2) - (1 + \frac{7}{6}w)(1 + \frac{1}{6}w)} \quad (2.8)$$

$$s = 2.5 \ln(1 + \frac{7}{6}w) + 3.5 \ln(1 + \frac{1}{6}w) - 3.5 \ln(1+w) \quad (2.9)$$

where

$$w = M^2 \sin^2\eta - 1 \quad (2.10)$$

The shock angle η is related to the coordinates as follows

$$\tan\eta = \left. \frac{dr}{dx} \right|_{\text{shock}} = \frac{r_\alpha + r_\beta}{x_\alpha + x_\beta} \Big|_{\text{shock}} \quad (2.11)$$

We have assumed a perfect gas with constant specific heats and hence that

$$p = \rho^\gamma \exp[(\gamma - 1)s] \quad (2.12)$$

It should be noted that this formulation eliminates the difficulty mentioned in the Introduction. For by using the (α, β) - coordinate system, a quantity such as

$$\frac{\partial p}{\partial \epsilon}(\alpha, \beta; \epsilon)$$

signifies the variation with ϵ at fixed α and β . In particular it gives the variation of pressure say fixed at the body or at the shock. This makes the integration of the differential equations significantly simpler.

VARIATIONAL EQUATIONS

As in Chapter 1, we differentiate the governing equations with respect to the parameter of interest, keeping the coordinates α and β held fixed. The differentiation although straightforward is tedious. If we write

$$\Theta = \frac{\partial \theta}{\partial \epsilon}, \quad S = \frac{\partial s}{\partial \epsilon}, \quad X = \frac{\partial x}{\partial \epsilon}, \quad R = \frac{\partial r}{\partial \epsilon}, \quad \Psi = \frac{\partial \mu}{\partial \epsilon} \quad (2.13)$$

and parametrically differentiate (2.1), (2.2), (2.3) and (2.5) we then obtain,

$$S_{\beta} = 0 \quad (2.14)$$

$$\begin{aligned} \Theta_{\alpha} + [P_{\mu\mu}(\mu) \mu_{\alpha} - \frac{s_{\alpha} \cos 2\mu}{\gamma} + \frac{r_{\alpha} \tan^2 \theta \sec^2 \mu}{r(\tan \theta + \tan \mu)^2}] \Psi + P_{\mu}(\mu) \Psi_{\alpha} - \frac{\sin 2\mu}{2} S_{\alpha} \\ + \frac{r_{\alpha} \sec^2 \theta \tan^2 \mu}{r(\tan \theta + \tan \mu)^2} \Theta - \frac{r_{\alpha} \tan \theta \tan \mu}{r^2(\tan \theta + \tan \mu)} R = 0 \end{aligned} \quad (2.15)$$

$$\Theta_{\beta} + \left[\frac{x_{\beta} \theta}{x_{\alpha}} \alpha \sec^2 \theta \tan \mu \right] \Theta - (1 - \tan \theta \tan \mu) \frac{x_{\beta}}{x_{\alpha}} \Theta_{\alpha} =$$

$$P_{\mu}(\mu) \Psi_{\beta} + [P_{\mu\mu}(\mu) \mu_{\beta} - \frac{x_{\beta} \theta}{x_{\alpha}} \sec^2 \mu \tan \theta + \frac{r_{\beta}}{r} \sec^2 \mu] \Psi \quad (2.16)$$

$$+ (1 - \tan \theta \tan \mu) \frac{\theta_{\alpha}}{x_{\alpha}} (X_{\beta} - \frac{x_{\beta}}{x_{\alpha}} X_{\alpha}) + \frac{\tan \mu}{r} R_{\beta} - \frac{r_{\beta} \tan \mu}{r^2} R$$

$$R_{\alpha} = X_{\alpha} \tan(\theta + \mu) + X_{\alpha} \sec^2(\theta + \mu)(\Theta + \Psi) \quad (2.17)$$

$$R_{\beta} = X_{\beta} \tan \theta + X_{\beta} \sec^2 \theta \quad (2.18)$$

At the shock the parametrically differentiated equations are

$$\begin{aligned} \frac{d\eta}{d\epsilon} = \frac{\cos^2 \eta}{(x_{\alpha} + x_{\beta})^2} \left[R_{\alpha}(x_{\alpha} + x_{\beta}) + R_{\beta}(x_{\alpha} + x_{\beta}) - X_{\alpha}(r_{\alpha} + r_{\beta}) \right. \\ \left. - X_{\beta}(r_{\alpha} + r_{\beta}) \right] \end{aligned} \quad (2.19)$$

$$S = \left[\frac{17.5}{6+7w} + \frac{3.5}{6+w} - \frac{3.5}{1+w} \right] \frac{dw}{d\epsilon} \quad (2.20)$$

$$\Psi = \frac{0.2A \left[\frac{4}{3} + \frac{7}{18} w \right] - 0.2 \left[1 + \frac{7}{6} w \right] \left[1 + \frac{1}{6} w \right] \left[0.2 M^2 - \frac{1}{3} - \frac{7}{18} w \right]}{A^2 \sin 2\mu} \frac{dw}{d\epsilon} \quad (2.21)$$

where $\frac{dw}{d\epsilon} = M^2 \sin 2\eta \frac{d\eta}{d\epsilon}$, $A = 1 + 0.2M^2(1+w) - (1 + \frac{7}{6}w)(1 + \frac{1}{6}w)$

$$\frac{d\theta}{d\epsilon} = \frac{d\eta}{d\epsilon} \cos^2 \theta \left\{ - \frac{1}{\sin^2 \eta} \frac{(M^2-1)\tan^2 \eta - 1}{(1 + \frac{\gamma+1}{2} M^2) + (1 + \frac{\gamma-1}{2} M^2) \tan^2 \eta} \right. \quad (2.22)$$

$$\left. + \frac{2}{[(1 + \frac{\gamma+1}{2} M^2) + (1 + \frac{\gamma-1}{2} M^2) \tan^2 \eta]^2} \left[(M^2-1) \sec \eta (1 + \frac{\gamma+1}{2} M^2) \right. \right. \\ \left. \left. + (1 + \frac{\gamma-1}{2} M^2) \tan^2 \eta \right] - [(M^2-1)\tan^2 \eta - 1] (1 + \frac{\gamma-1}{2} M^2) \sec^2 \eta \right\}$$

In the actual integration (2.18-2.22) are applied at the shock

$$\alpha = \beta \quad (2.23)$$

At the body $\alpha = 0$ the appropriate equations are

$$\underline{X} = 0, \quad \underline{R} = f \frac{\partial \beta}{\partial \underline{\epsilon}}, \quad \underline{\theta} = \frac{\partial f_{\beta}(\beta, \epsilon)}{\partial \underline{\epsilon}} \cos^2 \theta \quad (2.24)$$

In writing (2.24) we revert to the general case in which many parameters are being considered. Now we simultaneously numerically integrate the non-linear system and the variational equations. The calculation of the base flow is second order accurate [2]. The calculation of the new flow is first order in space, second order in the parameters of interest. The calculation of the two flows is interleaved in that after the flow along $\beta = 0$ constant is computed by the base code, the parametric code then calculates the exact derivatives in order to obtain the variational flow.

RESULTS

In the numerical calculations discussed, we have taken for f a family of shapes given by

$$r = 2\epsilon x(1-x) + 10x\epsilon(x-1)\left(x - \frac{1}{2}\right)c \quad (2.25)$$

Here we have taken ϵ to be the thickness ratio based on chord, and c as a scaling factor for the taper function.

Figure 3 shows the effect of changing just the thickness ($c = 0$). Here we have plotted the pressure distribution on the upper surface and the body which, for aesthetics, has the lower surface plotted as a reflection of the upper surface. Note that the method gives good agreement with the exact solution even when the new thickness is 50% more than the base thickness.

Figure 4 shows the effect of changing a combination of thickness, and taper. Here we see that, although the body configurations are markedly different, there is very good agreement between the parametrically generated pressure distribution and the exact pressure distribution for the new body.

INVERSE CASE

The method which has been presented also works quite well in the inverse or design problem where the pressure on the body is known, but the shape of the body shape is to be determined.

Using the Bernoulli equation and the perfect gas law one may show [1]

$$\mu = \sin^{-1} \left[\left[\frac{\gamma-1}{2} \frac{\exp\left(\frac{\gamma-1}{\gamma}(s + \ln\gamma p)\right)}{1 + \frac{\gamma-1}{2} M^2 - \exp\left(\frac{\gamma-1}{\gamma}(s + \ln\gamma p)\right)} \right]^{\frac{1}{2}} \right] \quad (2.26)$$

This when differentiated, yields

$$\Psi = \frac{(\gamma-1)^2}{2\gamma} \frac{\left(1 + \frac{\gamma-1}{2} M^2\right) \exp(w)}{\left[1 + \frac{\gamma-1}{2} M^2 - \exp(w)\right]^2 \sin^2 \mu} S = \frac{(\gamma-1)^2 \left(1 + \frac{\gamma-1}{2} M^2\right) \exp(w)}{2\gamma \left[1 + \frac{\gamma-1}{2} M^2 - \exp(w)\right]^2 \sin^2 \mu} \frac{d(\ln p)}{de} \quad (2.27)$$

Where

$$w = \frac{\gamma-1}{\gamma} (s + \ln p)$$

At the body, equation (2.6) is no longer valid since we are attempting to determine the shape of the body. Instead we must use (2.5) and (2.26). Therefore, the parametrically differentiated equations (2.24) must be replaced by (2.17), (2.18) and (2.27). The integration may now proceed as in the direct case [2]. The results of the variational calculations are presented in Figures 5 and 6. Notice that even for a 10% change in the logarithm of the pressure (corresponding to a 20% increase in thickness), the difference between the exact body shape and the computed shape is less than 1%.

FIGURE CAPTIONS

- Fig. 1 Body, C^+ characteristics, streamlines and C^- characteristics (dashed) in physical (x,y) plane, from [1].
- Fig. 2 Body, C^+ characteristics and streamlines in (α,β) plane.
- Fig. 3 Pressure distribution on 25% and 30% thick bodies at $M = 6$ and the respective bodies.
- Fig. 4 Pressure distribution on untapered, 25% thick body and 0.10 taper, 30% thick bodies at $M = 6$ and the respective bodies.
- Fig. 5 Inverse case: Pressure distribution on 25% and 30% thick bodies, $M = 4$ along with generated bodies. Dashed body is computed shape.
- Fig. 6 Inverse case: Pressure distribution on 25% and 30% thick bodies, $M = 6$ along with generated bodies. Dashed body is computed shape.

PHYSICAL PLANE

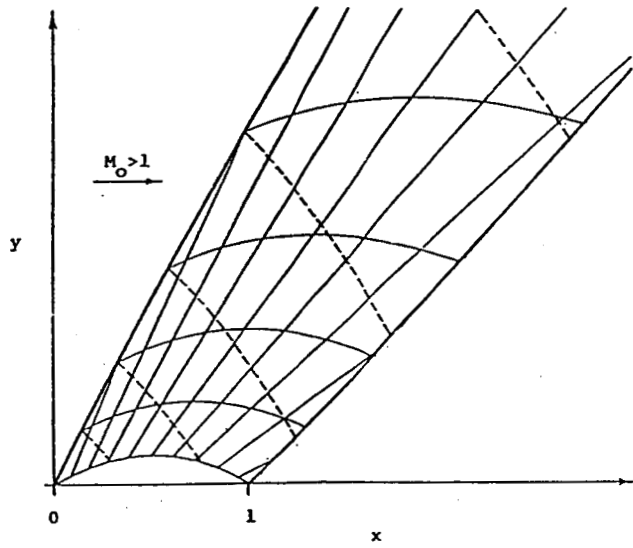


Figure 1

COMPUTATIONAL PLANE

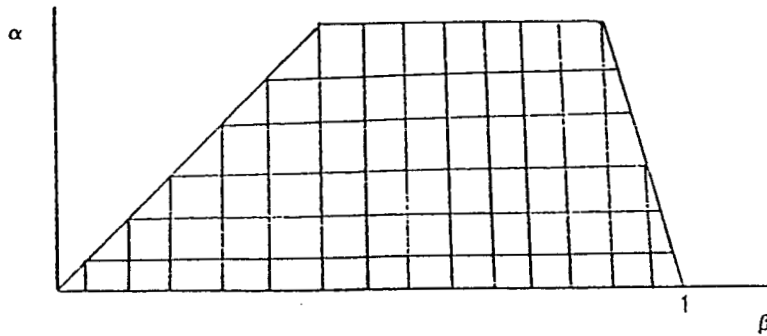
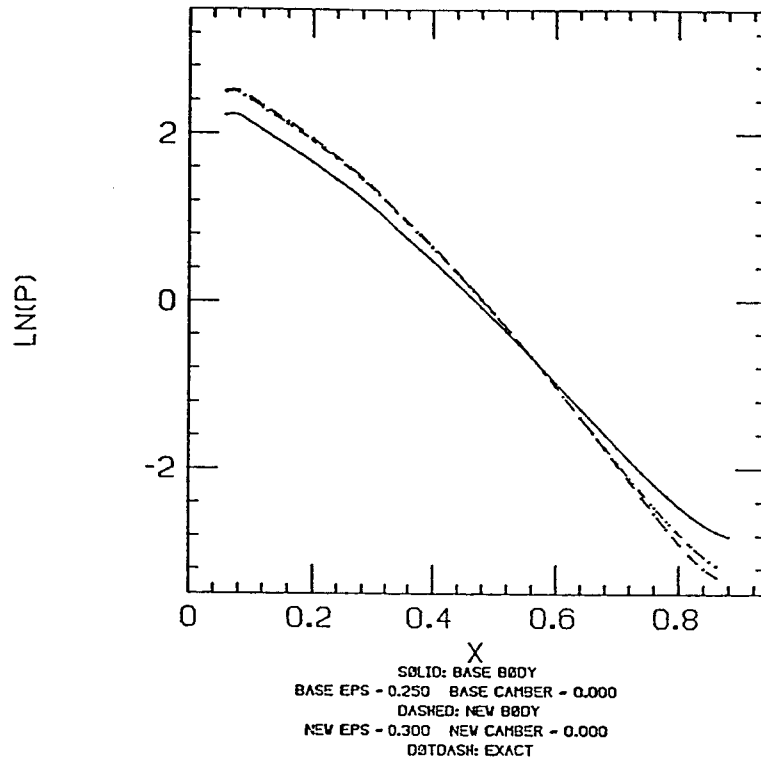


Figure 2

PRESSURE DISTRIBUTION ON BODIES $M_0 = 6.000$



BODIES

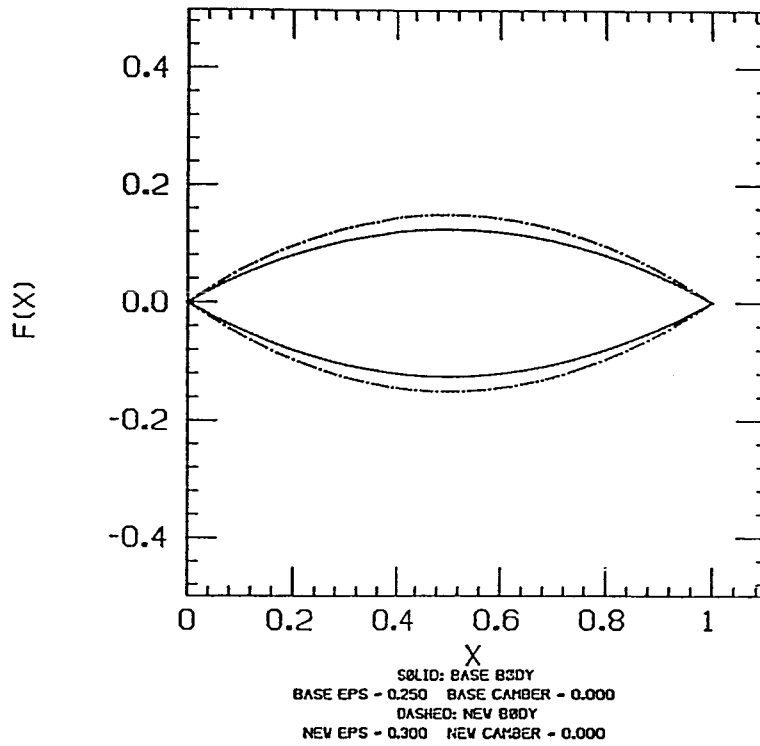
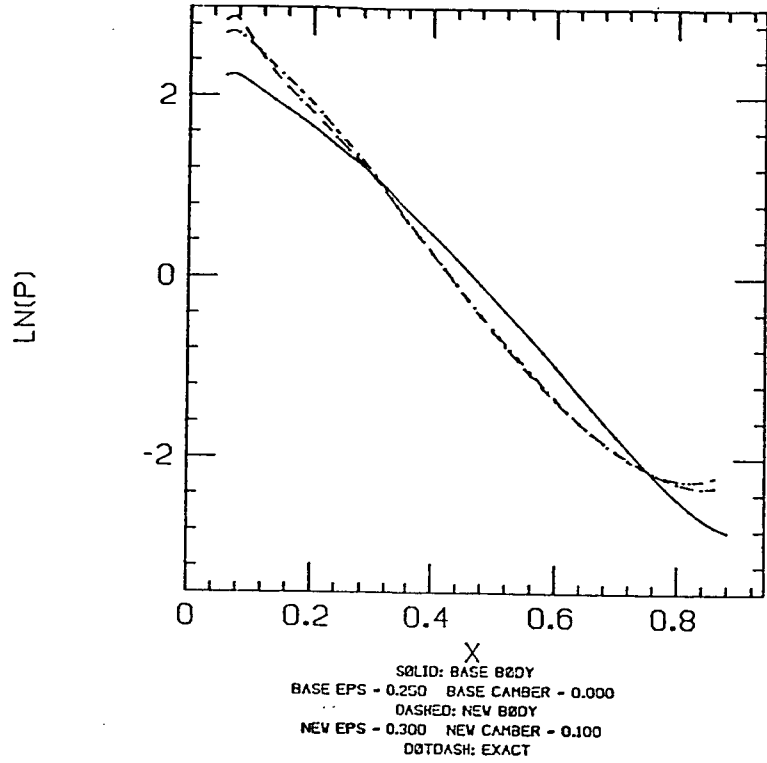


Figure 3

PRESSURE DISTRIBUTION ON BODIES MO - 6.000



BODIES

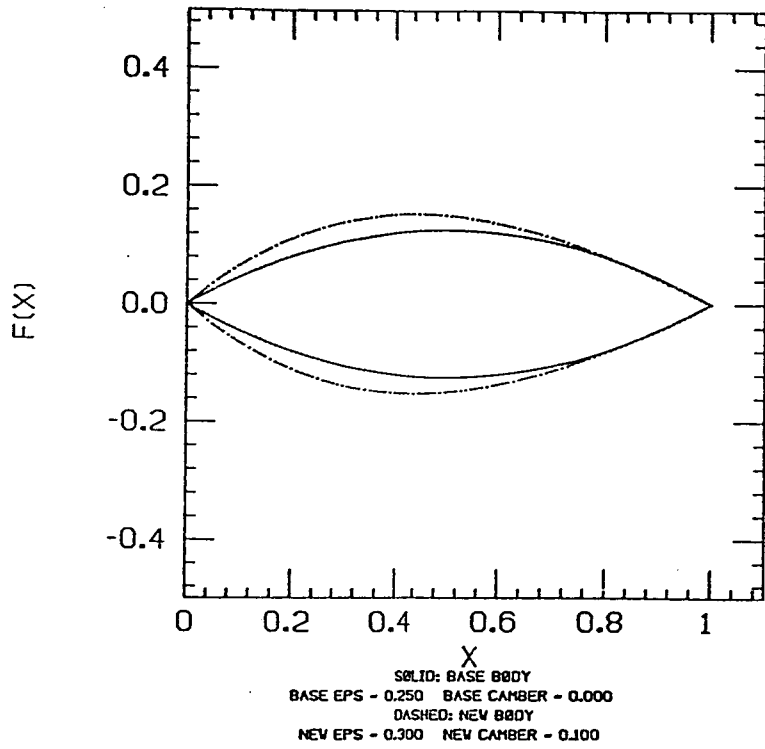


Figure 4

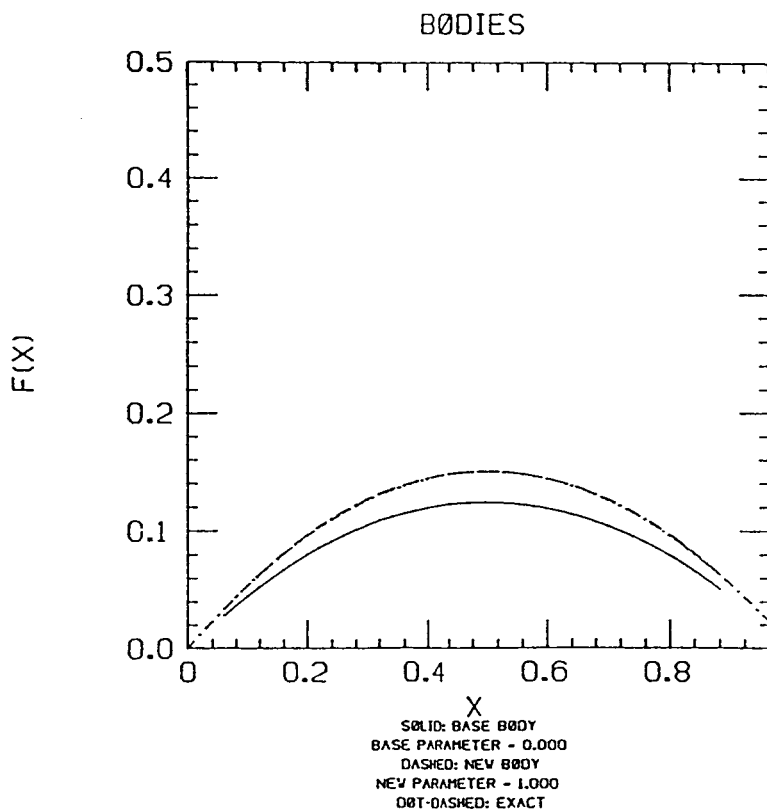
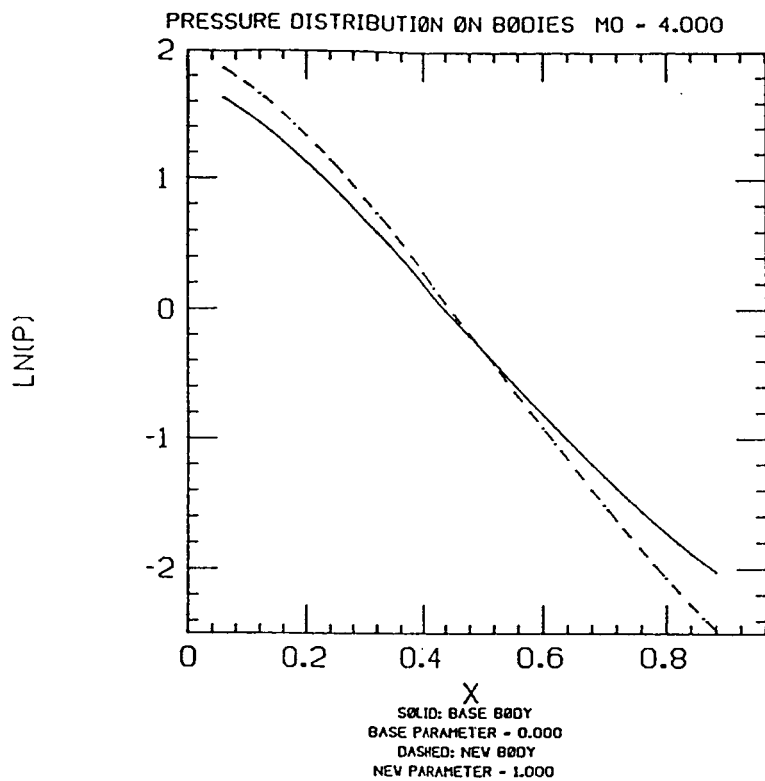
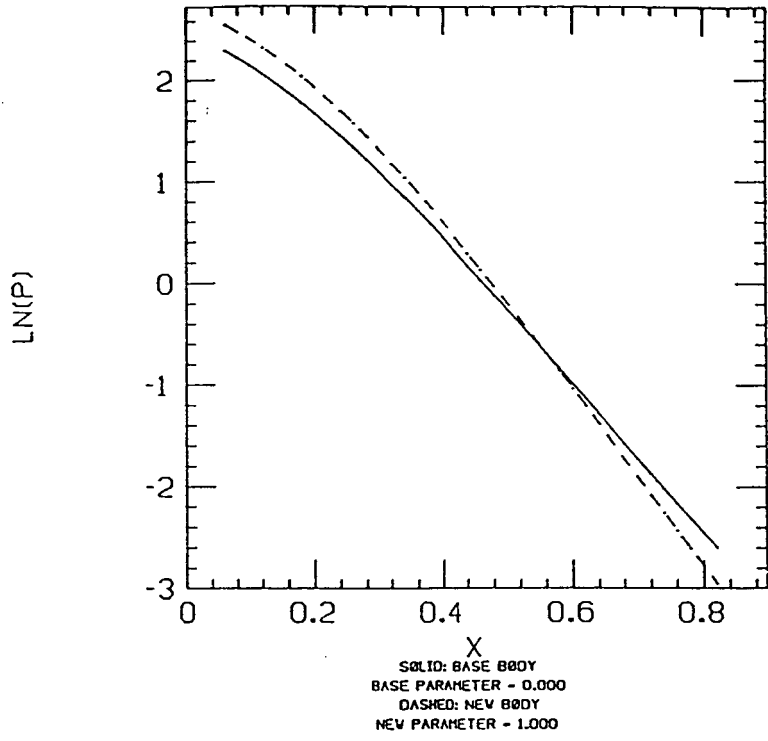


Figure 5

PRESSURE DISTRIBUTION ON BODIES MO - 6.000



BODIES

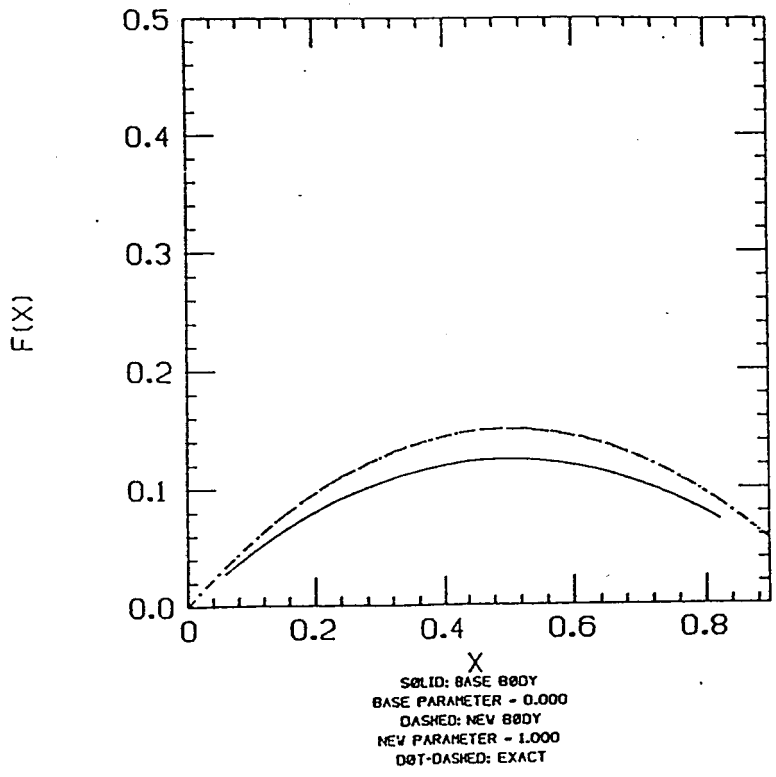


Figure 6

REFERENCES

- [1] Lewis, T.S. and Sirovich, L., "Approximate and Exact Numerical Computation of Supersonic Flow Over an Airfoil", J. Fluid Mechanics Vol 112, 1981, pp. 265-282.

- [2] Fong, J. and Sirovich, L. "Direct and Inverse Problem in Supersonic Axisymmetric Flow", AIAA Journal, 4, 5 May 1986.

Chapter III

The Jacobi Matrix Method for General Flows

Here one of the guinea-pigs cheered, and was immediately suppressed by the officers of the court.

- Alice's Adventures in Wonderland
Lewis Carroll

DIRECT DIFFERENCING

The procedure outlined in Chapters 1 and 2 holds in much greater generality than we have considered. The Jacobi matrix technique could also be applied to unsteady flows and to viscous flows in three dimensions. However, the method as presented so far, has one possible drawback which was alluded to earlier - to obtain the Jacobi matrix we must analytically differentiate the relevant equations and boundary conditions. In this chapter we propose a procedure which will allow for the calculation of the Jacobi matrix by the use of differential approximations. The goal is to obtain the Jacobi matrix, and hence be able to calculate a range of solutions in parameter space, using the results obtained from solving the nonlinear system (I.1) at only two distinct values of $\underline{\epsilon}$. This differential approach will be applied to the case of two dimensional supersonic flow considered in Chapter 1 and to two dimensional subsonic potential flow.

In the Introduction we said that if $\underline{u}^0 = \underline{u}(\underline{x}; \underline{\epsilon}_0)$ represented a known solution of the base flow then any neighboring flow at some fixed point \underline{x} is approximated by

$$\underline{u}(\underline{x}; \underline{\epsilon}) \approx \underline{u}^0 + \frac{\partial \underline{u}^0}{\partial \underline{\epsilon}_k} (\underline{\epsilon}_k - \underline{\epsilon}_0) \quad (3.1)$$

The obvious first order approximation for $\frac{\partial \underline{u}^0}{\partial \underline{\epsilon}_k}$ is

$$\left. \frac{\partial \underline{u}^0}{\partial \underline{\epsilon}_k} \right|_{\underline{x}, \text{ fixed}} \approx \left. \frac{\underline{u}(\underline{x}; \underline{\epsilon}) - \underline{u}^0}{\underline{\epsilon}_k - \underline{\epsilon}_0} \right|_{\underline{x}, \text{ fixed}} \quad (3.2)$$

What this says is that to compute $\frac{\partial \underline{u}^0}{\partial \underline{\epsilon}_k}$ we can take the value of \underline{u} at the location \underline{x} in the base flow and subtract it from the value of \underline{u} found from the perturbed flow ($\underline{\epsilon} = \underline{\epsilon}_0 + \Delta \underline{\epsilon}$) at the same location. In practice, this may require interpolation on one computational grid.

This approach requires special attention at a boundary. In our approach both material boundaries and possible shocks are taken to be boundaries and both give rise

to locations which change with $\underline{\epsilon}$. This would certainly be the case if we chose to vary the parameters of a body.

To be more specific, we would like to be able to use the calculation of pressure in the base flow in order to compute the pressure on the new body. Thus the formulas (1.25), (1.26) are no longer applicable since they apply at a fixed field point. Therefore, to correct (1.26) we must include changes in location of the body due to changes in $\underline{\epsilon}$. In the interests of simplicity we specify a three dimensional body by

$$y = f(x, z; \underline{\epsilon}) \quad (3.3)$$

A typical quantity, say pressure, at the new body, which we will specify by \underline{x}_0 , is related to the old body \underline{x}_0 in the following way

$$p(\underline{X}_0; \underline{\epsilon}) \approx p(\underline{x}_0; \underline{\epsilon}_0) + \frac{\partial p(\underline{x}_0; \underline{\epsilon}_0)}{\partial \epsilon_k} \cdot \Delta \epsilon_k + \frac{\partial p(\underline{x}_0; \underline{\epsilon}_0)}{\partial y_0} \frac{\partial f}{\partial \epsilon_k} \Delta \epsilon_k \quad (3.4)$$

where $\Delta \underline{\epsilon} = \underline{\epsilon} - \underline{\epsilon}_0$ and

$$\underline{x}_0 = (x_0, f(x_0, z_0; \underline{\epsilon}_0), z_0) \quad (3.5)$$

and

$$\underline{X}_0 = (x_0, f(x_0, z_0; \underline{\epsilon}), z_0) \quad (3.6)$$

Compare (3.4) with equation (1.26).

Note that we have related \underline{X}_0 to \underline{x}_0 by placing \underline{X}_0 directly above \underline{x}_0 in the x-z plane. Other choices are possible and may be more appropriate in certain cases.

Equation (3.4) in fact gives us the ability to compute the pressure at the new body, but requires knowledge of the differential coefficients $\frac{\partial p}{\partial \underline{\epsilon}}$. They can be obtained from

$$\frac{\partial p(\underline{x}_0; \underline{\epsilon}_0)}{\partial \epsilon_k} \approx \frac{p(\underline{X}_0; \underline{\epsilon}) - p(\underline{x}_0; \underline{\epsilon}_0) - \frac{\partial p(\underline{x}_0; \underline{\epsilon}_0)}{\partial y_0} \frac{\partial f}{\partial \epsilon_k} \Delta \epsilon_k}{\Delta \epsilon_k} \quad (3.7)$$

to first order, or

$$\frac{\partial p(x_0; \epsilon_0)}{\partial \epsilon_k} \approx \frac{p(x_0; (\epsilon + \epsilon_0)/2) - p(x_0; \frac{3\epsilon_0}{2} - \frac{\epsilon}{2})}{\Delta \epsilon_k} - \frac{\partial p(x_0; \frac{3\epsilon_0}{2} - \frac{\epsilon}{2})}{\partial y_0} \frac{\partial f}{\partial \epsilon_k} \quad (3.8)$$

It should be noted that the differential determination of the differential coefficient $\frac{\partial p}{\partial \epsilon}$ requires not only calculation of the different flow fields, but also of $\frac{\partial p}{\partial y_0}$. Therefore, in the numerical calculation it is necessary to compute $\frac{\partial p}{\partial y_0}$ at the body. This we do by interpolation.

To illustrate these remarks we return to the case treated in Chapter 1. We consider two dimensional supersonic flow at thicknesses of 10% and 10.1% to calculate $\frac{dx}{d\epsilon}$, $\frac{dy}{d\epsilon}$, $\frac{d\theta}{d\epsilon}$, $\frac{d\mu}{d\epsilon}$, $\frac{ds}{d\epsilon}$. Using equation (3.8) the resulting derivatives were then used to compute the pressure distribution on a 15% thick airfoil (Figure 1). Note that this pressure distribution compares favorably with that computed from using the Jacobi matrix generated by solving the differential equations (Chapter 1, Figure 3). The error between the two computations is less than 1%.

2D SUBSONIC FLOW

As a second illustration we apply the Jacobi matrix technique to the potential equation for two dimensional compressible flow. The potential equation is derived by assuming inviscid, irrotational flow and is valid for subsonic flows and for low transonic flows when boundary layer effects can be neglected.

Since we have implemented the Jacobi technique by modifying Jameson's computer code FLO36 we will summarize the derivation of the relevant equations and their solution [1],[2].

Under the assumption of irrotational flow we may introduce a velocity potential ϕ such that

$$u = \phi_x \quad v = \phi_y \quad (3.9)$$

The potential satisfies the quasilinear equation

$$(a^2 - u^2) \phi_{xx} - 2uv \phi_{xy} + (a^2 - v^2) \phi_{yy} = 0 \quad (3.10)$$

where a is the local speed of sound. When given the ratio of specific heats γ , the stagnation speed of sound a_0 and the local speed $q = \sqrt{u^2 + v^2}$ the speed of sound is determined by

$$a^2 = a_0^2 - \frac{\gamma-1}{2} q^2 \quad (3.11)$$

We will consider (3.10) for subsonic flows. (But see Figure 9 for a transonic case).

At the body the flow must satisfy the tangency condition

$$\frac{\partial \phi}{\partial n} = 0 \quad (3.12)$$

where n is the normal derivative and the Kutta condition - that the tangential velocity is bounded at the trailing edge. In the far field the potential approaches the potential of a vortex in compressible flow and a uniform stream. The density and pressure are determined by relations

$$p\gamma^{-1} = M_\infty^2 a^2 \quad (3.13)$$

and

$$p = \frac{p^\gamma}{\gamma M_\infty^2} \quad (3.14)$$

The coordinate system used for computation is generated by conformally mapping the exterior of the airfoil to the interior of the unit circle. The airfoil itself becomes the coordinate line $r = 1$ (Figure 2).

Since the far field boundary condition must now be applied at $r = 0$, where the

potential becomes infinite, a reduced potential which removes this singularity is introduced by

$$G = \phi - \frac{\cos(\theta + \alpha)}{r} + E(\theta + \alpha) \quad (3.15)$$

Here α is the angle of attack and $2\pi E$ is the circulation.

If the modulus of the transformation from the physical plane to the circle plane is denoted by H then (3.10) becomes

$$\begin{aligned} (a^2 - u^2)G_{\theta\theta} - 2uvrG_{r\theta} + (a^2 - v^2)r \frac{\partial}{\partial r}(rG) \\ - 2uv(G_{\theta} - E) + (u^2 - v^2)rG_r + (u^2 + v^2) \left(\frac{u}{r} H_{\theta} + vH_r \right) = 0 \end{aligned} \quad (3.16)$$

The u and v are the velocity components in the θ and r directions, respectively and are given by

$$u = \frac{r(G_{\theta} - E) - \sin(\theta + \alpha)}{H}, \quad v = \frac{r^2 G_r - \cos(\theta + \alpha)}{H} \quad (3.17)$$

The Neumann boundary condition (3.12) becomes

$$G = \cos(\theta + \alpha) \text{ at } r = 1 \quad (3.18)$$

while the far field condition is

$$G = E\{\theta + \alpha - \tan^{-1} [\sqrt{1 - M_{\infty}^2} \tan(\theta + \alpha)]\} \text{ at } r = 0 \quad (3.19)$$

The circulation is determined by the Kutta condition which requires that the velocity be finite at the trailing edge of the airfoil. Here we have $H = 0$ and $\phi_{\theta} = 0$ so (3.15) reduces to

$$E = G_{\theta} - \sin\alpha \text{ at } r = 1, \theta = 0 \quad (3.20)$$

The details of the calculation of H and of the multigrid solution of (3.16)-3.20)

are not essential for our purposes and are discussed in references [1], [3], [4], [5]. The important point is that the transformation to the circle plane is conformal so that every airfoil in the physical plane is mapped to a circle and every physical flow is mapped to the interior of the circle.

CALCULATION OF THE JACOBI MATRIX

The equations for computing the Jacobi matrix by finite differences were given by equations (3.4)-(3.8). In the subsonic case the only parameter changed was the airfoil thickness based on chord. Due to the construction of equation (3.16) the quantities which are of interest are the reduced potential G , and the metric H . To define the locations \underline{x} in equation (3.2) we note that in the circle plane the points are spaced angularly (θ) as $2\pi/(\text{the number of grid points about airfoil})$ and radially (r) as $1/(\text{the number of grid points from airfoil to far field})$. Therefore, it is natural to define the location \underline{x} by the intersection of these lines.

The variational flow was computed using essentially the same procedure which was used to calculate the pressure in the two dimensional supersonic flow case. In the transformed plane we first compute the flow about an airfoil of thickness ϵ_1 and save the converged values of G and H . Next we compute the flow about an airfoil of thickness ϵ_0 . We use these computed values of G and H along with those from the run at thickness ϵ_1 to compute $\frac{dG}{d\epsilon}$ and $\frac{dH}{d\epsilon}$ using (3.7). G and H for the variational flow at thickness ϵ is computed using equation (3.4).

RESULTS

Figure 3 shows the results of a parametric calculation using a base airfoil of 10% thickness based on chord and a second airfoil of 10.1% thickness to predict the pressure distribution on a 14% thick airfoil. It should be noted that there is very close agreement between the parametric calculation and the solution given by FLO36.

Figure 4 uses a 10% thick airfoil and 10.1% thick airfoil to calculate the flow

over 15% thick profile - that is, a profile which is 50% more than the base airfoil. Again the agreement is quite good. Figures 5 through 8 show the same calculations for flows at different Mach numbers. All show close agreement between the parametrically generated solutions and those given by FLO36.

The method breaks down when there is a drastic change in the behavior of the solution in the parameter space. This is illustrated in Figure 9. Here the flows about the 10% and 10.1% thick airfoils are subsonic but the flow about the 15% thick airfoil is supercritical. The method is unable to account for the shock.

FIGURE CAPTIONS

- Fig. 1. Pressure distribution on 10% and 15% thick airfoils at $M = 4$ calculated by direct differencing along with respective bodies.
- Fig. 2. Computational plane, from [2].
- Fig. 3. Pressure distribution on 14% thick airfoil, $M = 0.75$. Solid curve is FLO36 result, dashed is parametric. Base and new airfoils are also shown.
- Fig. 4. Pressure distribution on 15% thick airfoil, $M = 0.75$. Solid curve is FLO36 result, dashed is parametric. Base and new airfoils are also shown.
- Fig. 5. Pressure distribution on 14% thick airfoil, $M = 0.60$. Solid curve is FLO36 result, dashed is parametric. Base and new airfoils are also shown.
- Fig. 6. Pressure distribution on 15% thick airfoil, $M = 0.60$. Solid curve if FLO36 result, dashed is parametric. Base and new airfoils are also shown.
- Fig. 7. Pressure distribution on 14% thick airfoil, $M = 0.45$. Solid curve is FLO36 result, dashed is parametric. Base and new airfoils are also shown.
- Fig. 8. Pressure distribution on 15% thick airfoil, $M = 0.45$. Solic curve is FLO36 result, dashed is parametric. Base and new airfoils are also shown.
- Fig. 9. Pressure distribution on 15% thick airfoil, $M = 0.80$. Solid curve is FLO36 results, dashed is parametric. Base and new airfoils are also shown.

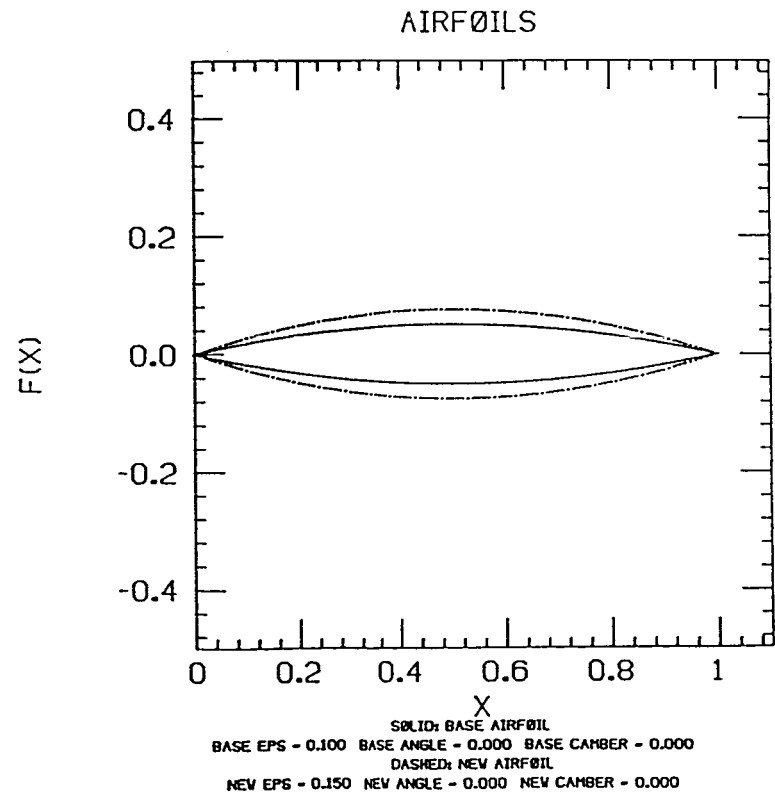
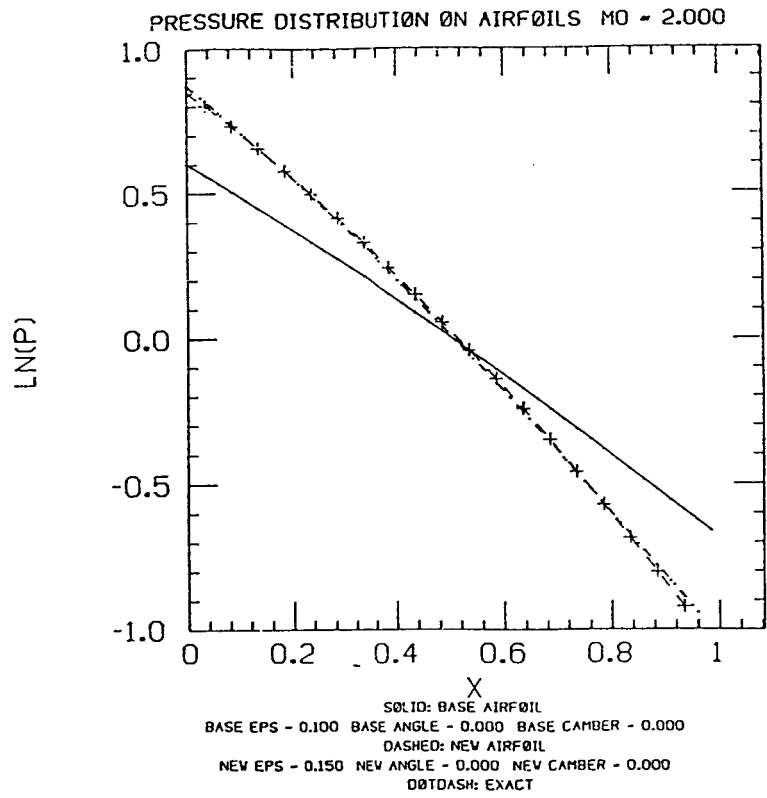


Figure 1

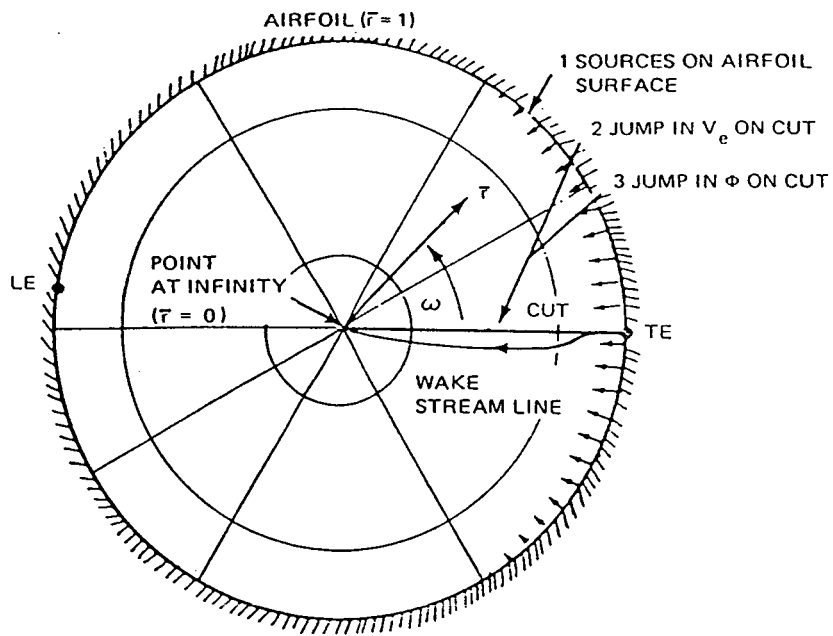


Figure 2

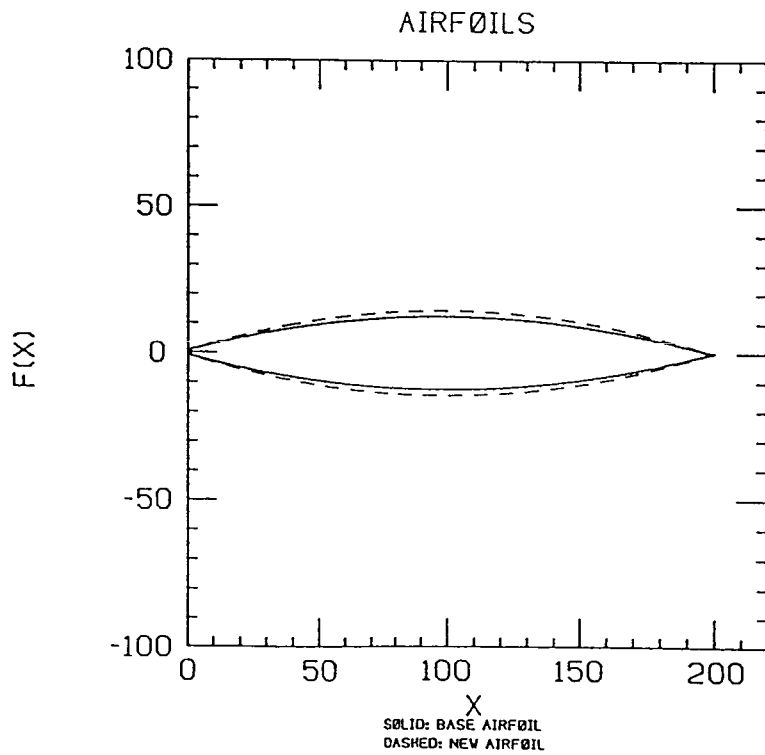
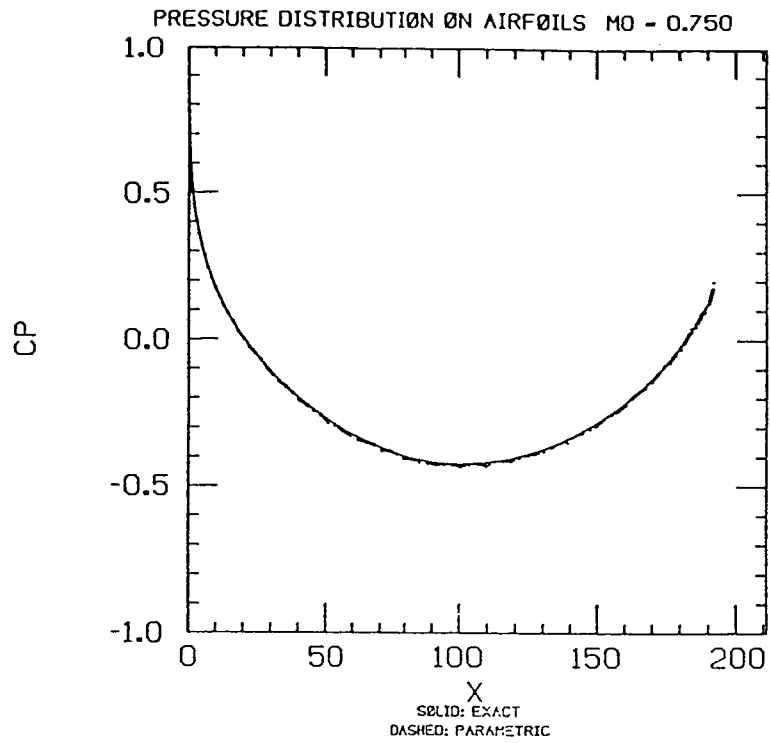


Figure 3

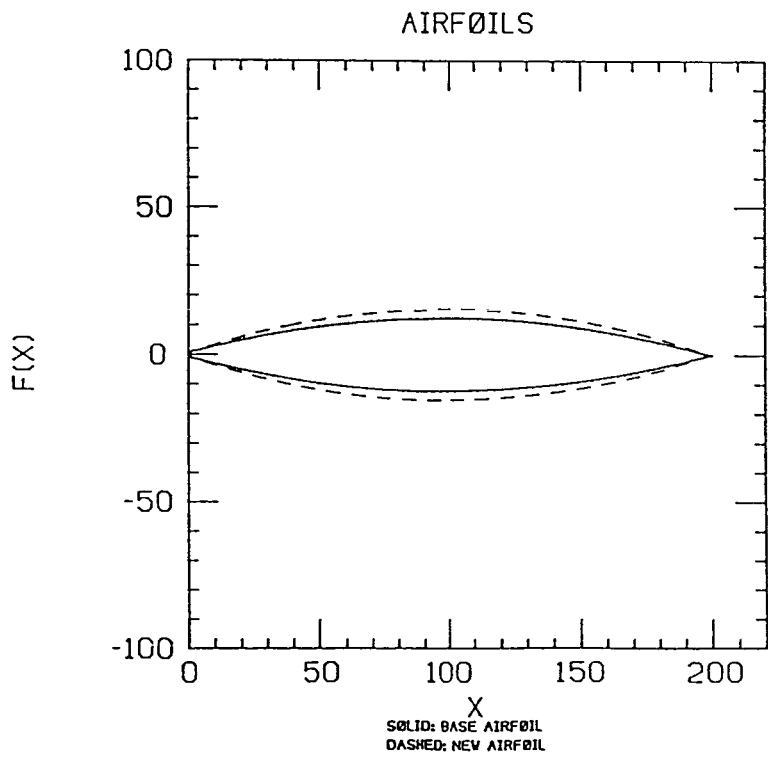
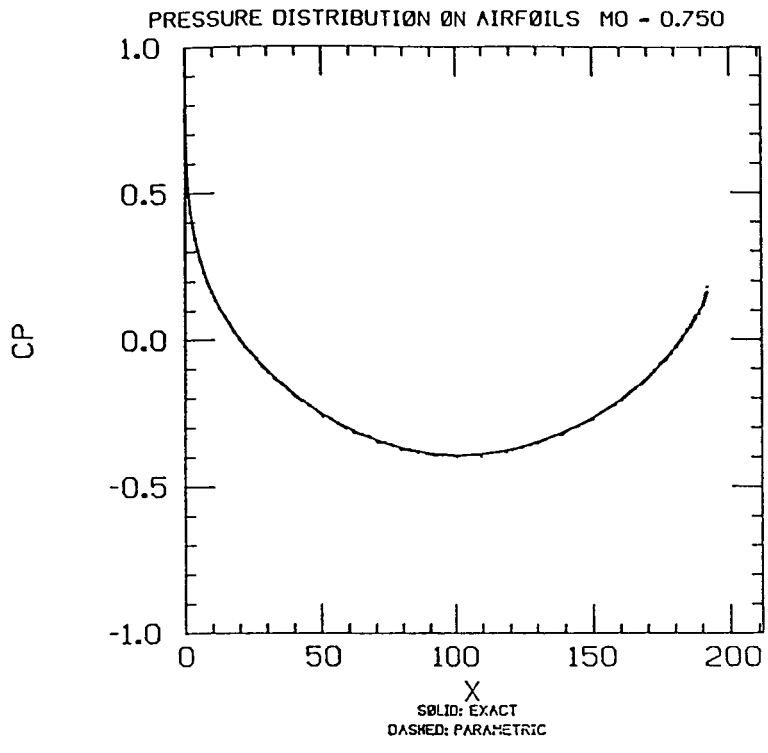


Figure 4

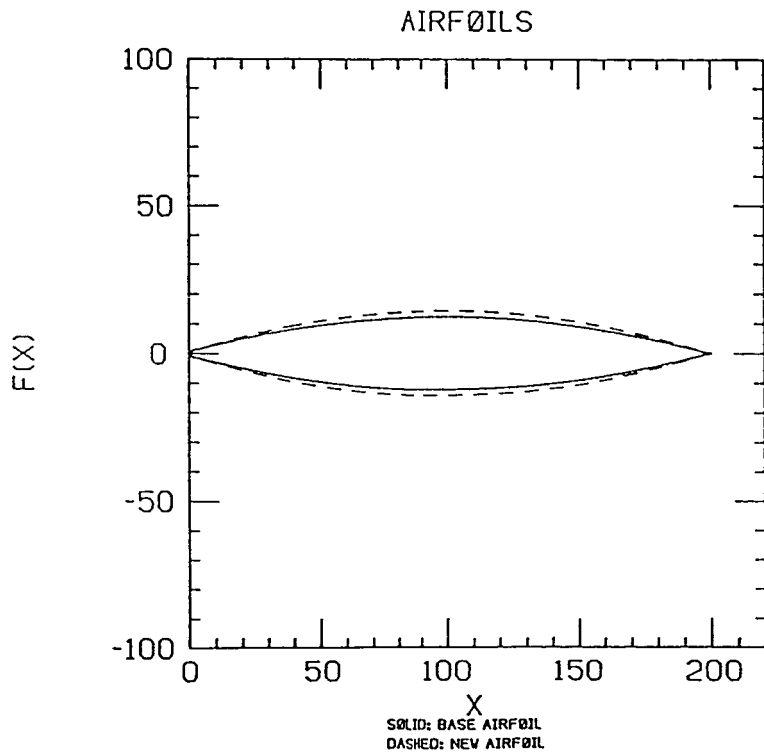
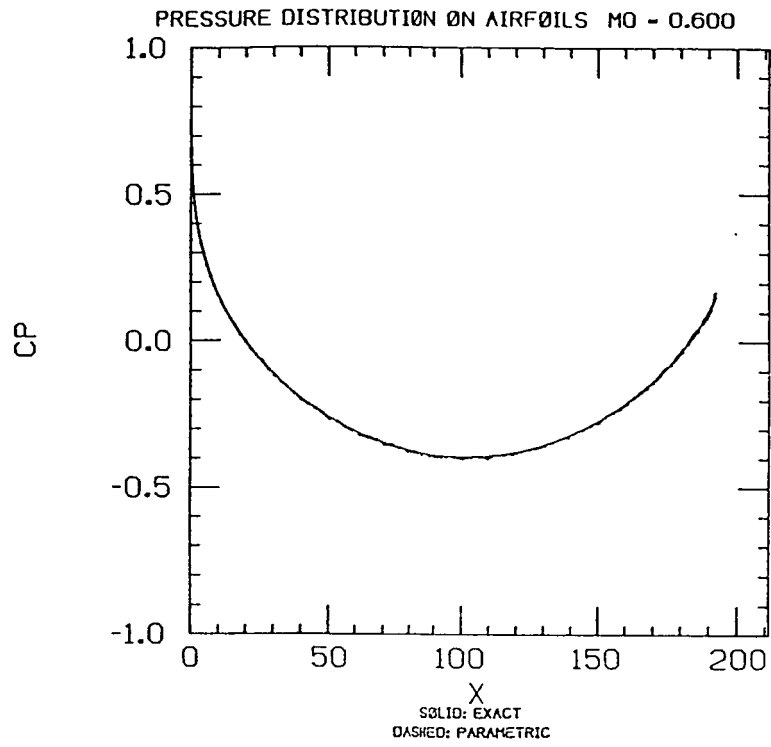


Figure 5

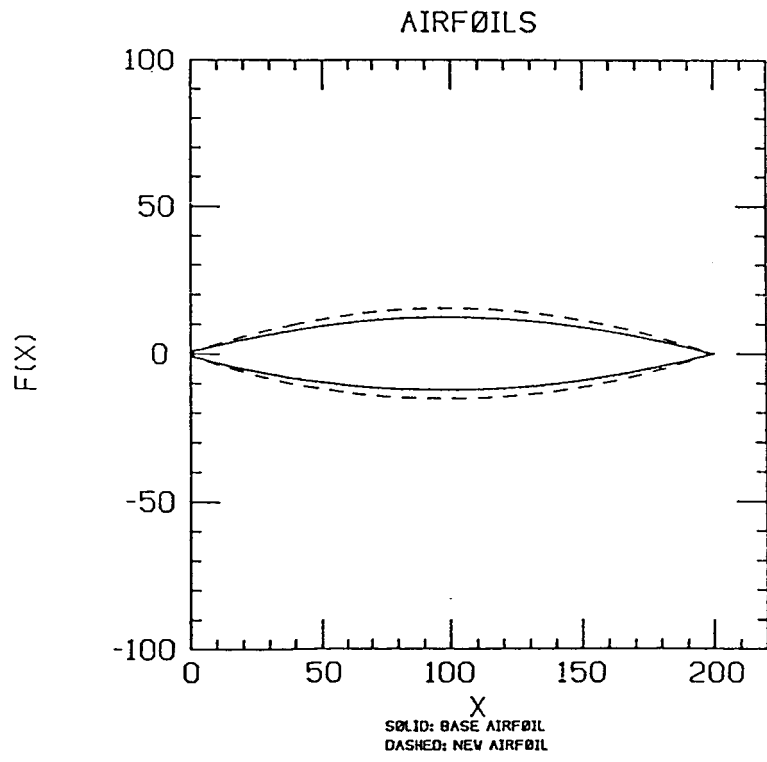
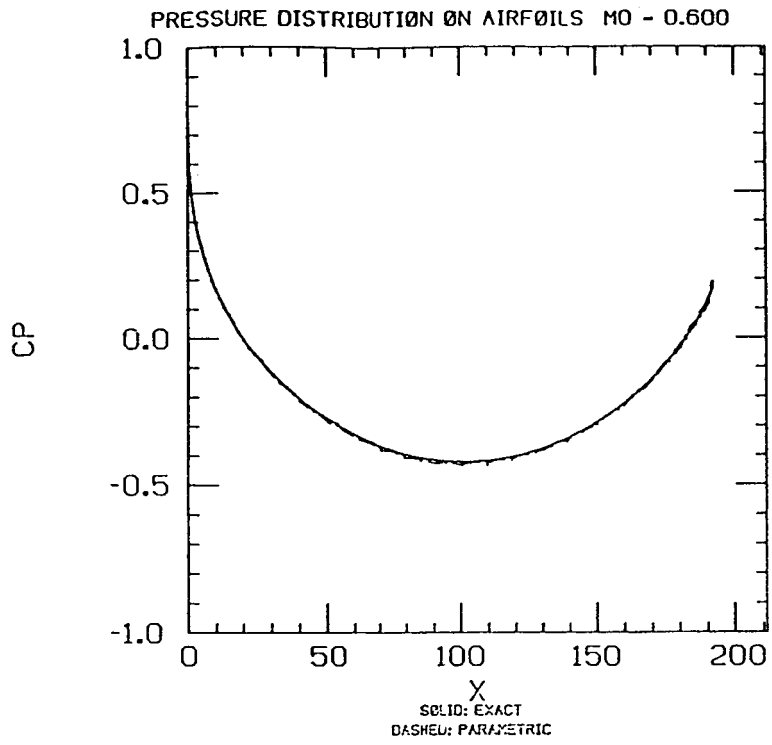


Figure 6

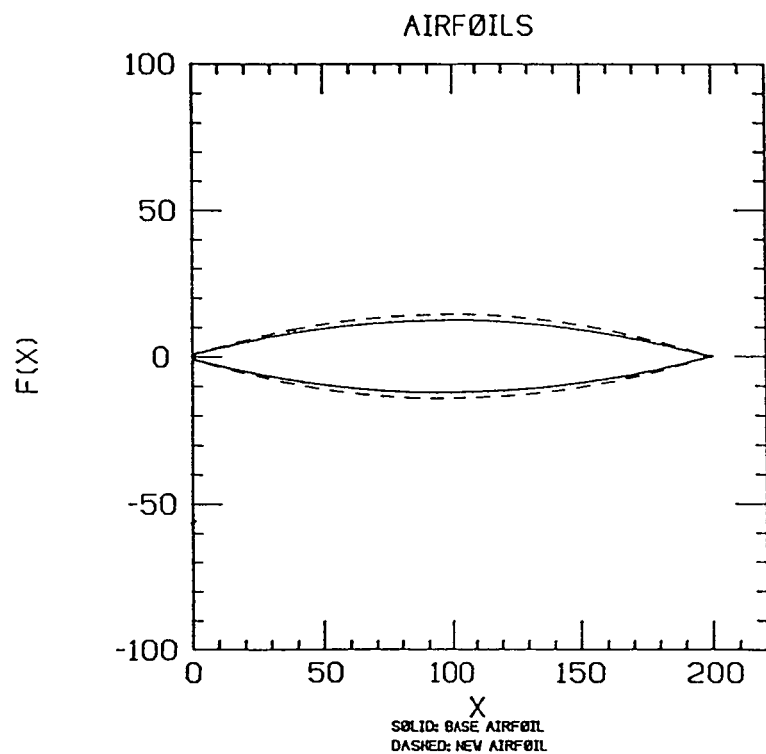
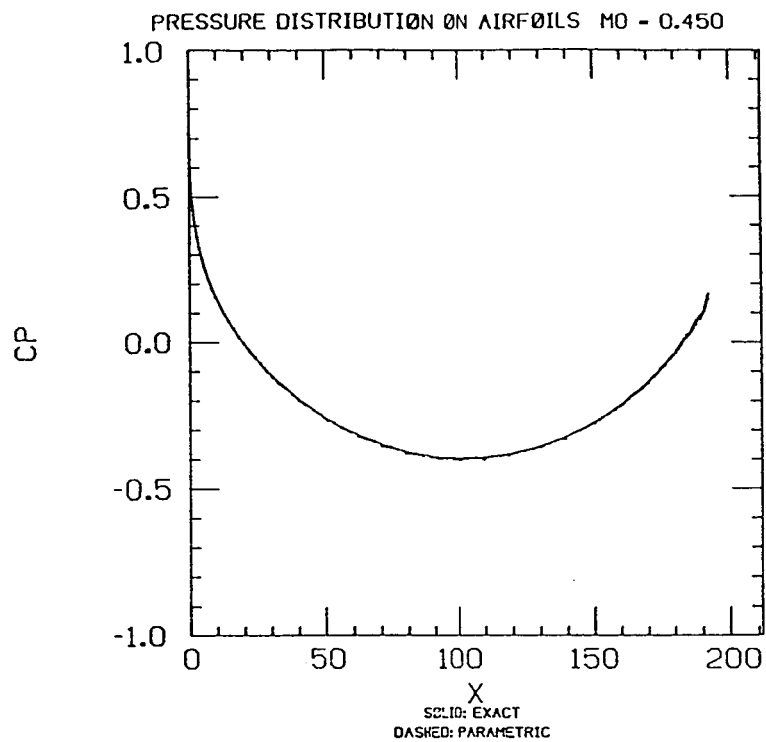


Figure 7

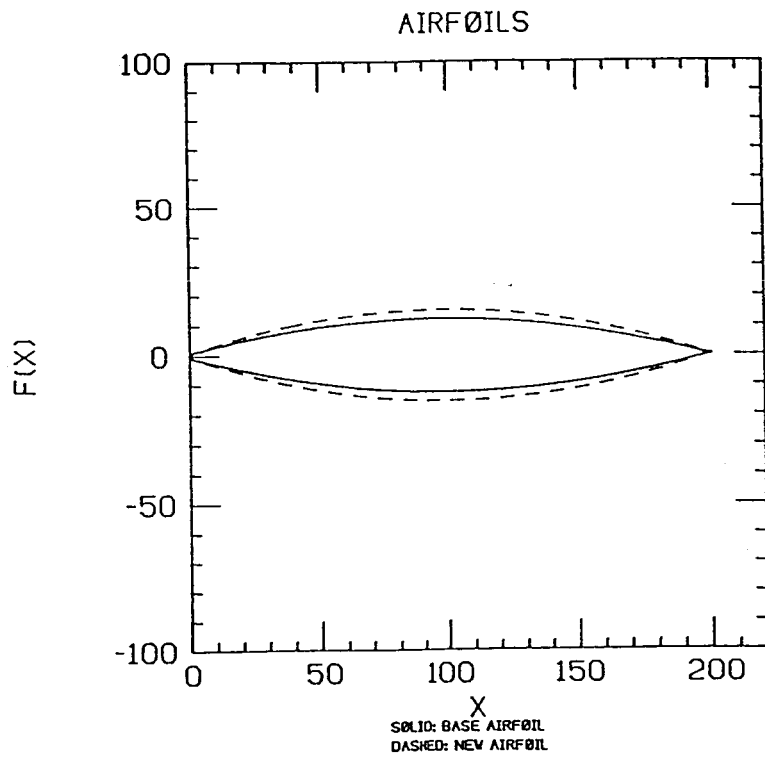
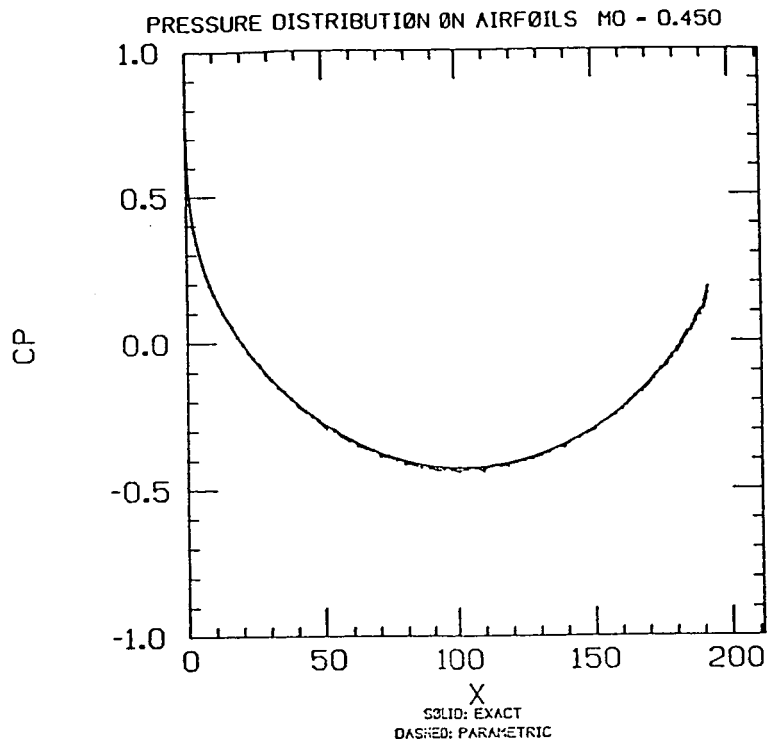


Figure 8

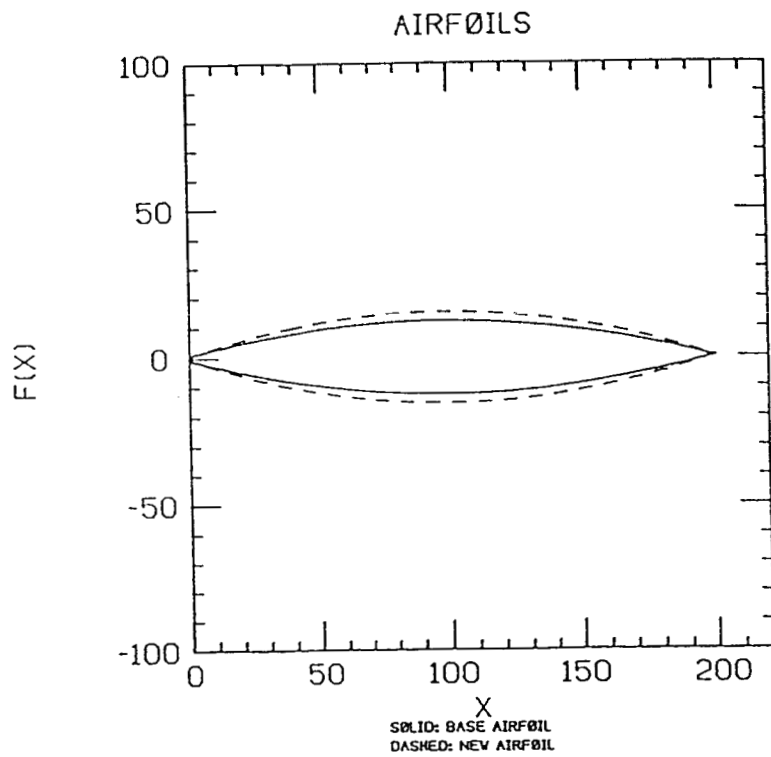
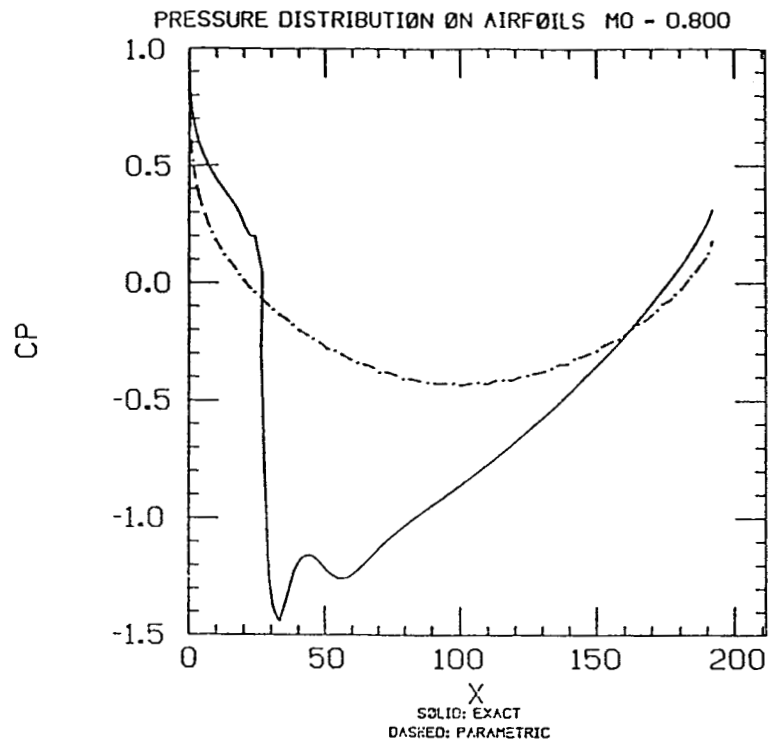


Figure 9

REFERENCES

- [1] Jameson, Antony, "Acceleration of Transonic Potential Flow Calculations on Arbitrary Meshes by the Multiple Grid Method", AIAA 79-1458
- [2] Melnik, R.E., Chow, R.R., Mead, H.R., Jameson, A., "An Improved Viscid/Inviscid for Transonic Flow Over Airfoils", NASA CR-3805, 1985.
- [3] Jameson, Antony, "Transonic Flow Calculations" in Wirz, H.J. and J.J. Smolderen (ed), Numerical Methods in Fluid Dynamics, McGraw-Hill Book Co., 1978.
- [4] Bauer, F., Garabedian, P., Korn, D., Jameson, A., "Supercritical Wing Section II", Springer-Verlag, New York, 1975.
- [5] Jameson, Antony, "Transonic Flow Calculations", Lecture Notes, Courant Institute of Mathematical Sciences, New York, 1976.
- [6] Jameson, Antony, "The Evolution of Computational Methods in Aerodynamics", MAE Report No. 1608, May 1983.